

Review

Seabed Dynamic Responses Induced by Nonlinear Internal Waves: New Insights and Future Directions

Tian Chen ^{1,2} , Zhenghui Li ¹, Hui Nai ³, Hanlu Liu ¹, Hongxian Shan ^{1,4} and Yonggang Jia ^{1,4,*}

¹ Shandong Provincial Key Laboratory of Marine Environment and Geological Engineering, Ocean University of China, Qingdao 266100, China

² Key Laboratory of Coastal Science and Integrated Management, Ministry of Natural Resources, Qingdao 266061, China

³ School of Earth System Science, Tianjin University, Tianjin 300072, China

⁴ Laboratory for Marine Geology, Qingdao National Laboratory for Marine Science and Technology, Qingdao 266061, China

* Correspondence: yonggang@ouc.edu.cn

Abstract: Strong nonlinear internal waves generate a significant pressure force on the seafloor and induce a pore-pressure response penetrated in the seabed and are thus an important driver of sediment resuspension and a potential trigger of seabed failure. The following provides an overview of the seabed responses induced by nonlinear internal waves and the theory, models, and limited observations that have provided our present knowledge. The pressure disturbance is generated by the combined effect of interface displacement and near-bottom acceleration by the nonlinear internal waves. Recent observations in the South China Sea have shown that the pressure magnitudes up to 4 kPa, which is the largest known disturbance. Intense pore-pressure changes in roughly the top 1 m of the weakly conductive seabed are expected during the shoaling and breaking of the nonlinear internal waves and lead to 2 cm sediments of the local seabed appearing in transient liquefaction. Since the fluid seepage reduces the specific weight of the bed, results show that the contribution of vertical seepage on sediment resuspension is estimated at 11% for a seabed saturation of 0.97. Finally, in situ observations are needed to confirm theoretical knowledge and to help improve our ability to model the multiscale interaction process between the seabed and internal waves in the future.

Keywords: internal solitary waves; seabed stability; pore pressure; dynamic response; seepage



Citation: Chen, T.; Li, Z.; Nai, H.; Liu, H.; Shan, H.; Jia, Y. Seabed Dynamic Responses Induced by Nonlinear Internal Waves: New Insights and Future Directions. *J. Mar. Sci. Eng.* **2023**, *11*, 395. <https://doi.org/10.3390/jmse11020395>

Academic Editor:
George Kontakiotis

Received: 14 December 2022
Revised: 29 January 2023
Accepted: 3 February 2023
Published: 10 February 2023



Copyright: © 2023 by the authors. Licensee MDPI, Basel, Switzerland. This article is an open access article distributed under the terms and conditions of the Creative Commons Attribution (CC BY) license (<https://creativecommons.org/licenses/by/4.0/>).

1. Introduction

Nonlinear internal waves (NLIWs) are a large-amplitude short-period fluctuation that occur in the interior of the stratification ocean [1,2]. Internal solitary waves (ISWs) are a particular type of NLIW that appear frequently, in which the wave structure is isolated, propagation is unidirectional, and the velocity and waveform remain essentially constant during propagation [3,4]. One type of NLIW that is found in the upper ocean depresses the isopycnals and hence is referred to as a depression wave. Another type of NLIW elevates the isopycnals that are located in the bottom half of the ocean and hence is referred to as an elevation wave [5–7]. NLIWs are widely observed in the global oceans, such as the South China Sea [8,9], the Andaman Sea [10], the Massachusetts Bay [11], and the New Jersey's Shelf [12], among many others (Figure 1a).

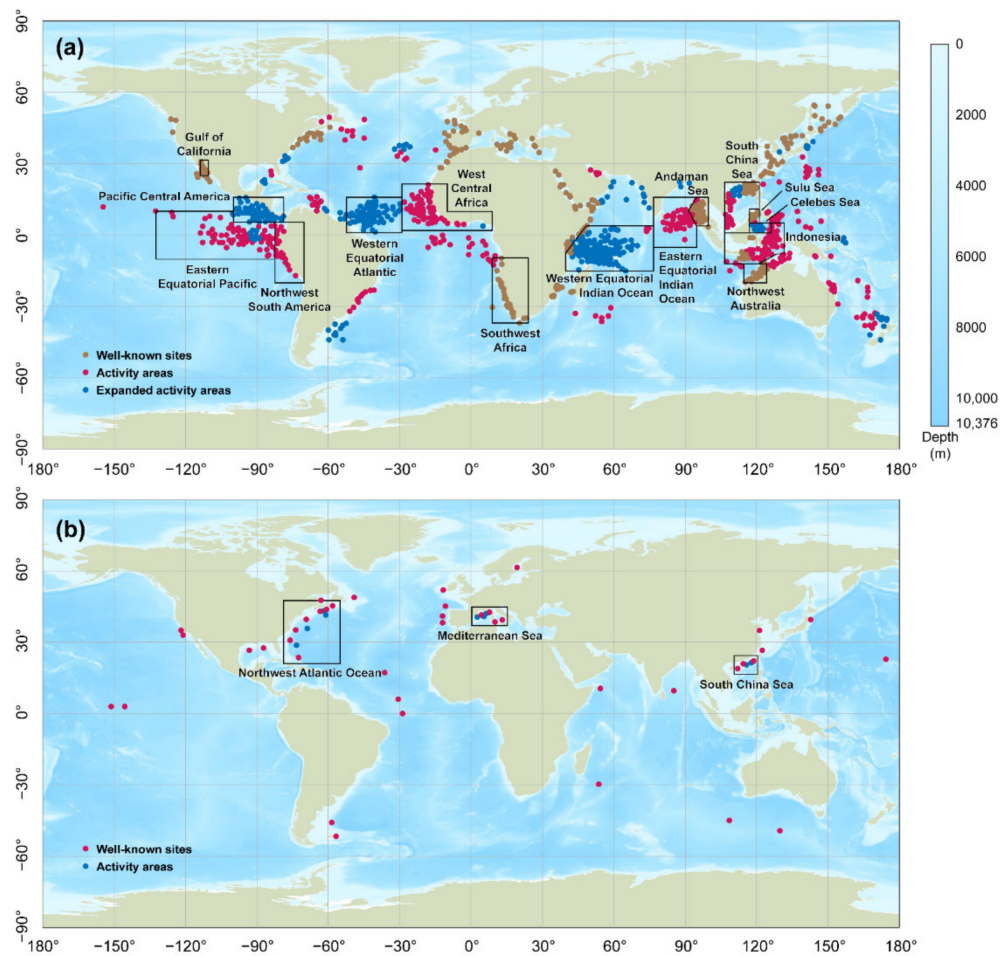


Figure 1. Nonlinear internal wave and nepheloid layer distribution around the world. (a) Global internal waves observed in MODIS imagery from 2002 through 2004, adapted from Jackson [13]. (b) Global nepheloid layers observed from 1953 through 2019, adapted from Tian et al. [14]. The well-known sites are regions where internal waves or nepheloid layers have been previously reported and their characteristics well-documented. The activity areas are regions where internal wave or nepheloid layer activity has been reported but their characteristics have not been determined. The expanded activity areas are regions in which the MODIS survey found a significant amount of internal wave activity where little or no activity had been previously reported.

Typically, NLIWs have wavelengths more than tens of kilometers long, amplitudes often exceed 200 m, and periods last from tens of minutes to several hours [2]. The strongest ISWs in the world were reported by Huang et al. [15] in the South China Sea, with amplitudes exceeding 240 m and a westward current reaching 2.55 m/s. On the one hand, NLIWs induce bottom shear stress [16] and benthic boundary layer instability [2], which may become sufficient for particle initiation and sediment resuspension, especially during ISW shoals in the continental shelf and slope [17,18], where the powerful nepheloid layers were often observed (Figure 1b). On the other hand, NLIWs are capable of inducing significant pressure (positive or negative) upon the seafloor [19,20] and excess pore pressure [21–23] in the sediment during their passage, whether they are depression waves or elevation waves. The pore pressure is the fluid pressure (liquid pressure and gas pressure) in the seabed pore space. In addition, pore fluid circulation and seepage appear in the strong pore-pressure gradient zone beneath the seafloor, the enhanced sediment resuspension, and the driving bottom nepheloid layer burst events [21,22]. Understanding this relationship is necessary, since changes in seabed stability and sediment resuspension potentially modify the submarine topography [19,24], the solute transport across the sediment-water interface [25], and the biogeochemical cycles [26].

Sediment resuspension and transport by NLIWs receive the most attention and benthic boundary layer instability driven by NLIWs is believed to be the principal mechanism [2,17]. During NLIW propagation, the observation data at 2000 m depth showed that the acoustic backscattering intensity of the benthic boundary layer was enhanced, velocities exceeded 0.6 m/s and the suspended particulate matter concentration increased by two orders of magnitude and reached 14.3 mg/L above 7.9 m of the bottom [27]. Much of what has been inferred about bottom shear stress generated by NLIWs and their effects in eroding and transporting sediment is taken from extensive compilation results of field observations, theoretical inference, numerical simulation, and laboratory experiments [16,28–30]. Unfortunately, individual research data provide little or no information about the seabed dynamic response of NLIW events and they have rarely been coupled with direct measurements of seafloor pressure or seabed pore pressure.

Conductivity, stiffness, and saturation are important mechanical properties of sediments [21,31]. The stiffness and saturation dictate how the pressure that waves exert on the seafloor is transmitted through the sediments with a fine material of weak conductivity and eventually cause the seabed dynamic responses [32], even the seabed instability. Surface waves, including solitary surface waves, have been identified as the occurrence of wave-induced seabed effective stress attenuation so far as to liquefaction [33]. For an unsaturated seabed with a small amount of gas, only a deep trough wave that induces strongly negative bottom pressure can be generating powerful seepages vertically from the seabed, then eroding and resuspending the sediment [34]. However, in deep-sea environments with depths greater than 200 m, the effect of surface waves on the seabed is extremely weak [21]. The NLIWs, whose amplitudes are 20–30 times larger than that of surface waves under the same energy conditions, can generate significant perturbations in the deep sea bottom [35]. The study of the dynamic response mechanism of the seabed under the action of NLIWs is of great significance for engineering safety and geohazard forecasts [36,37].

It is noteworthy to note that pore pressure has long been recognized by researchers as a crucial aspect of marine geohazards [38]. The earliest known attempt to measure pore pressures in submarine sediments was made by Lai et al. [39]. Since then, Richards et al. [40] first discussed the effect of pore pressures caused by the NLIW-cyclical loading of the seafloor. NLIW shoaling and breaking could cause cyclical wave pressure [41,42], which may cause changes in soil behavior. These ideas about patterns of seabed dynamic responses induced by NLIWs have been supported by subsequent numerical models and field measurements [21–23]. The first numerical investigation work to explore the interaction between the internal wave and the elastic seabed of a porous medium was by Chen and Hsu [23]. For the highly nonlinear ISWs of the depression type, the pore-pressure field has been examined using numerical simulations [21]. Not until the late 2000s and early 2010s were time-series measurements of bottom high-accuracy pressure transducers made simultaneously with a moored acoustic doppler current profiler (ADCP) [12,20,43]. Episodic response in NLIW-induced pressure in the ocean was first documented in long-time series measurements (1.5-month duration) using a Paroscientific Model 6000-200A pressure transducer moored on the seafloor on the New Jersey shelf [43]. The first known used submarine piezometer to acquire ISW-induced pore pressure was by Ocean University of China (OUC). These authors describe a differential FBG-Piezometer that was designed to operate in water depths of up to 3500 m [44]. Richards et al. [40] hypothesized that the NLIWs induced seabed dynamic responses; since then numerous studies have contributed to understanding their effect and mechanism. Nonetheless, major questions remain: How intense, variable, or persistent are NLIW-induced seabed dynamic responses? How do pore fluid circulation and seepage affect sediment resuspension? Are high-frequency internal waves required to both initiate and maintain the buildup of pore pressure or have NLIWs generated seabed strength weakening and triggered geohazards?

In this paper, we first review known characteristics of NLIW-induced pressure structure (theoretical and numerical results, as well as the field observation data) in Section 2. The time-series bottom pressure measurements were obtained in months' long deployments

of a pressure transducer and other moorings. We compare the different bottom pressure records of existing studies to gain a perception on major questions. We then investigate how the pore pressure (Section 3) and fluid seepage (Section 4) variations of the seabed relate to NLIWs. Section 5 provides a conclusion and future outlook on these issues. Our results provide important new insights into the intense, variable, and persistent NLIW-induced seabed dynamic responses. Because pore fluid circulation carries nutrients and trace elements into the benthic boundary layer [45], our results also provide key information that will be useful to submarine biogeochemical processes where pore pressure is critical for understanding NLIW–seabed interactions.

2. The Pressure Disturbance of the Seafloor

During the NLIW propagation, the seafloor pressure disturbance is a significant cause of seabed pore-pressure dynamic response, which is also reflected in the magnitude of perturbation of the NLIW–seabed interaction [21]. The pressure of NLIWs on the seafloor has been the subject of gradually intensive investigations, through both theoretical analysis and numerical simulations, supplemented in more recent years by in situ observations based on high-precision pressure sensors. All these methods are complementary and are illustrated in the following subsections.

2.1. Theoretical and Numerical Results

2.1.1. Wave-Pressure Structure of the Bottom

Theoretically, bottom pressure disturbance caused by NLIWs has been investigated previously as a problem in density and velocity changes of the water column [23,43,46,47]. As mapped by Moum and Smyth [46], the wave pressure structure of the seafloor consists of three components (as in Figure 2):

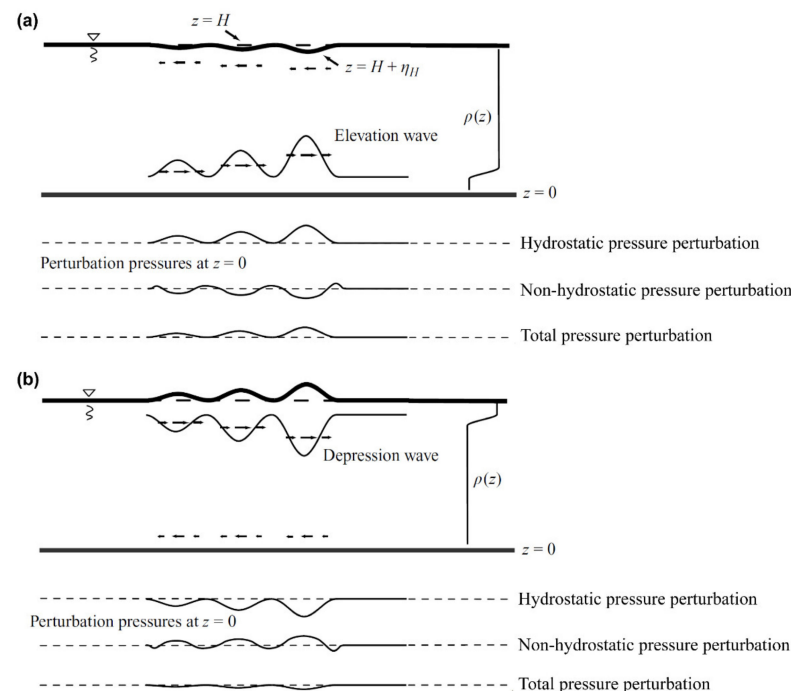


Figure 2. Schematic bottom pressure structure induced by NLIWs. (a) Comparable between surface wave displacement, hydrostatic pressure, non-hydrostatic pressure, and total pressure in an NLIW train of elevation propagating to the right. The black arrows show the relative velocity of the wavefronts and induced near-surface velocity. (b) A similar structure for NLIW train of depression propagating to the right. Panels (a,b) adapted from Moum and Smyth [46], with permission from Cambridge University Press.

- a. An internal hydrostatic pressure perturbation as a result of the NLIW-driven isopycnals displacement, which for depression or elevation waves are negative or positive pressure, respectively.
- b. An external hydrostatic pressure perturbation as a result of the free surface fluctuation, related to near-surface velocity convergence and divergence that is driven by NLIWs, which for depression or elevation waves are positive or negative pressure, respectively.
- c. A non-hydrostatic pressure perturbation as a result of NLIW-driven near-seabed accelerations in the vertical, which for depression or elevation waves are dominated by positive or negative pressure, respectively.

2.1.2. Governing Equations for Wave Forcing

In the pioneering work of Chen and Hsu [23], the two-layer interfacial wave system (as in Figure 3) with inviscid and irrotational assumption was considered for solving the NLIW–seabed interaction problem. In this study, the upper layer is assumed to be a free surface and the lower layer is assumed to be a rigid boundary (i.e., as a seabed). Moreover, the NLIW motion $\eta_2(x, t)$ and free surface fluctuation $\eta_1(x, t)$ is specified as simple harmonic motion. Chen and Hsu [23] considered the independent velocity potential ϕ in both layers. Moreover, the internal wave pressure equation is deduced based on the superposition principle which was previously used to solve the boundary value problem of the complex conditions of the interaction between the surface wave and the seabed [48].

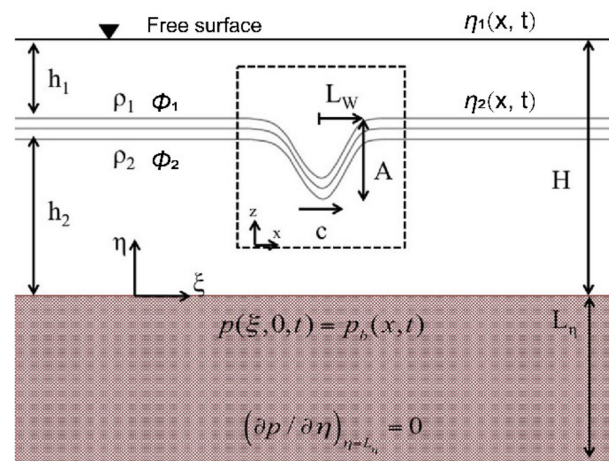


Figure 3. Typical definition sketch of a two-layer fluid system for a depression ISW propagating over a flat seabed. The seabed thickness L_η , the ISW amplitude A , half-wavelength L_w , and a phase speed c are also shown. The ISW lies in a reference frame, x - z , that moves with the wave. The bed lies in a fixed reference frame, ξ - η . The boundary conditions of the porous medium come from Rivera-Rosario et al. [21]. Figure adapted from Rivera-Rosario et al. [21], with permission from Wiley.

According to Chen and Hsu [23], the internal wave pressures $P_{Chen \ \& \ Hsu}$ at the seafloor ($z = 0$) is expressed as

$$P_{Chen \ \& \ Hsu} = \frac{1}{2} p_0 \text{Re} \left[\left(e^{i(kx - \sigma t)} + e^{i(kx + \sigma t)} \right) \right], \tag{1}$$

where Re is the function real part and $i = \sqrt{-1}$ stands for the imaginary part of a complex variable. p_0 is related to the bottom pressure to the first order of the wave theory, which is given by

$$p_0 = -\rho_w \left(\sum \dot{\phi}_j \right), \tag{2}$$

where ρ_w is the fluid reference density, $j = (1, 2)$ represents the upper layer and the lower layer, and $(\dot{\cdot})$ stands for the time differentiation. The final form for the p_0 can be expressed as

$$p_{0,1} = -\rho_1 \dot{\phi}_1 = -\frac{\rho_w b \sigma^2}{k} \left\{ \frac{gk \cosh kd - \sigma^2 \sin h kd}{gk \sinh kh_1 - \sigma^2 \cosh kh_1} \right\}, \tag{3}$$

$$p_{0,2} = -\rho_2 \dot{\phi}_2 = \frac{b \rho_w}{k \rho_2} \left\{ \frac{[-gk \rho_2 \sigma^2 \cosh kh_1 + (g^2 k^2 (\rho_2 - \rho_1) + \rho_1 \sigma^4) \sinh kh_1]}{(gk \sinh kh_1 - \sigma^2 \cosh kh_1)} \cosh kh_2 + \frac{(\rho_2 \sigma^4 \cosh kh_1 - gk \rho_2 \sigma^2 \sinh kh_1)}{(gk \sinh kh_1 - \sigma^2 \cosh kh_1)} \sinh kh_2 \right\}, \tag{4}$$

where $p_{0,1}$ is the bottom pressure induced by free surface fluctuation $\eta_1(x, t)$ in the upper layer, $p_{0,2}$ is the bottom pressure induced by internal wave motion $\eta_2(x, t)$ in the lower layer, h_1 and h_2 are the water depth for the upper layer and lower layer, respectively, b is the amplitudes of the internal wave, ρ_1 and ρ_2 are the water density in the upper layer and lower layer, respectively, k is the internal wave number that is solved by a new wave dispersion relationship, and ϕ_1 and ϕ_2 are the velocity potential in the upper layer and lower layer, respectively (Figure 3).

In the equation of the internal wave pressures proposed by Chen and Hsu [23], the internal wave and the free surface perturbation have been assumed to be a linear wave (i.e., the wave amplitudes are small compared with the wavelength). In the same assumption, Williams and Jeng [47] showed the attenuation of internal wave propagation in a porous elastic seabed. However, unlike Chen and Hsu [23], Williams and Jeng [47] suggested that the velocity potential ϕ_1 in the upper layer does not affect the seafloor and only the velocity potential ϕ_2 of the lower layer is required to address the wave pressure problems. Furthermore, they extended the solution to the second-order nonlinear terms of the wave theory to understand the influence of the internal wave with finite amplitude on the porous seabed. According to Williams and Jeng [47], the internal wave pressures $P_{Williams \& Jeng}$ at the seafloor ($z = 0$) are expressed as

$$P_{Williams \& Jeng} = \sum_{n=1}^{\text{II}} A^{(n)} e^{in(kx - \omega t)}, \tag{5}$$

where $A^{(n)}$ stands for the high-order pressure amplitude of the internal wave motion and the superscripts I and II represent the order of approximation.

The above model regarding internal wave pressure derived by both Chen and Hsu [23] and Williams and Jeng [47] has not been supported by laboratory scale or field scale measurements and must be reviewed in more detail. In fact, the assumption of small amplitudes is not an accurate description of NLIWs with large amplitude features [49–51] and would give rise to a significant underestimation of seabed dynamic responses by NLIWs [21]. Moum and Smyth [46] revisited the problem using elevation NLIW forms modeled by the Korteweg de Vries (KdV) equation, despite the KdV equation being in accordance with the weakly nonlinear theory. In this study, the pressure model is derived from the vertical and horizontal components of the momentum equations, associated with a two-dimensional nonlinear non-hydrostatic internal wave, based on a non-rotating inviscid Boussinesq fluid assumption.

According to Moum and Smyth [46], the NLIW pressures $P_{Moum \& Smyth}$ is expressed as

$$P_{Moum \& Smyth} = p_U + p_{Wh} + \rho_0 g \eta_H + p_{nh}, \tag{6}$$

where p_U is the ambient profile pressure, p_{Wh} is the NLIW-driven disturbance pressure, $\rho_0 g \eta_H$ is the external hydrostatic pressure, and p_{nh} is the non-hydrostatic pressure. The p_U , p_{Wh} , η_H , and p_{nh} are written as

$$p_U = \int_z^H (\rho_0 + \rho_U) g \, dz, \tag{7}$$

$$p_{Wh} = \int_z^H \rho_w g \, dz, \tag{8}$$

$$\eta_H = -\frac{1}{g} \int_{-\infty}^x \frac{Du_H}{Dt} dx, \tag{9}$$

$$p_{nh} = \rho_0 \int_z^H \frac{Dw}{Dt} dz, \tag{10}$$

respectively, where ρ_0 is the reference density, $\rho_0 + \rho_U$ represents the ambient density profile, and where ρ_w is the NLIW-driven perturbation density, η_H is the free surface displacement, and u_H represents the wave propagation velocity. These models about the pressure of NLIWs have been supported by subsequent in situ measurements [46] and are validated in detail by Moum and Nash [43]. The highly sensitive pressure sensors provide details of wave pressure dynamics and subsequently filter raw time series of pressure required to extract the pressure signal of NLIWs. The computation of the bottom pressure signal of an NLIW from measurements of density and velocity is compared with the in situ observed pressure data to verify the correctness of the equation [43]. While it is widely known that the wave amplitude based on the KdV equation compared with the large amplitude observed in the field is too narrow [3,52], the fundamental pressure mechanism suggested by Moum and Smyth [46] is trusted to hold. Following the numerical methods given by Moum and Smyth [46], Rivera-Rosario et al. [21] revisited the issue by employing large-amplitude ISW described by the fully nonlinear Dubriel-Jacotin-Long (DJL) equation; both depression and elevation wave- types were considered.

Theoretical pressure models are useful for understanding the impact of NLIWs on the seabed and further pore-pressure response can be calculated. Compared to $P_{Moum \ \& \ Smyth}$, both $P_{Chen \ \& \ Hsu}$ and $P_{Williams \ \& \ Jeng}$ take a small amplitude linear internal wave assumption in with a two-layer simplified within the water column. In this way, a two-layer system simplifies the governing equations to accelerate the calculation time but introduces a greater uncertainty in the quantification of the NLIW pressures. In contrast, $P_{Moum \ \& \ Smyth}$ is more suitable for simulating large-amplitude NLIW pressures in the continuously stratified water column of real marine environments. However, for $P_{Moum \ \& \ Smyth}$, the assumption that without a change of NLIW form limits the estimation of pressure during wave breaking or wave mode transformation, as well as waveform inversion and for NLIW propagation with mode-2. Although theoretical and numerical results may guide seabed dynamic responses, direct application to the ocean to predict changes in the seafloor must be conducted with caution.

2.1.3. Characteristics of Wave-Pressure Disturbance

Based on the pressure structure of NLIWs shown in Figure 2, the wave pressure is dominated by internal hydrostatic pressure perturbation, whether it is a depression-wave type or an elevation-wave type [22,46]. Furthermore, the combination of external hydrostatic pressure perturbation and non-hydrostatic pressure perturbation always creates a negative contribution to the wave pressure, reducing the amplitude of the total pressure [43,46] and weakening the disturbance effect of NLIWs on the seafloor [21]. For depression NLIWs, these signs are reversed (Figure 2b). The wave pressure structures of depression NLIWs and elevation NLIWs have opposite mirror features [43,46].

As mapped by Moum and Smyth [46], the pressure disturbance on the seafloor is controlled by internal hydrostatic pressure perturbation, that is to say, the greater the NLIW amplitudes, the greater the wave pressure generated (Figure 4a). However, in other numer-

ical studies, simple linear correlations between NLIW amplitudes and seafloor pressures were not as expected. Rivera-Rosario et al. [21] investigated the dependency between the maximum ISW amplitude that is permissible and the wave pressure to determine which environmental parameter scheme gains the largest response. Numerical parameterized results show a significant pressure decrease when the ISW amplitude increases (i.e., changing $h_1/h_2 = 1/7$ to $h_1/h_2 = 1/10$, h_1/h_2 represents the ratio of upper and lower water depths) considering the different ratios of pycnocline thickness δ_{pyc} (the pycnocline thickness is defined as the thickness of the water column in which the density transition occurs) and water depth H (as shown in Figure 4b). They argued that higher amplitude ISWs also produced a simultaneously higher non-hydrostatic pressure which was associated with variations of fluid vertical motions. The non-hydrostatic pressure reduced the total ISW pressure on the bottom.

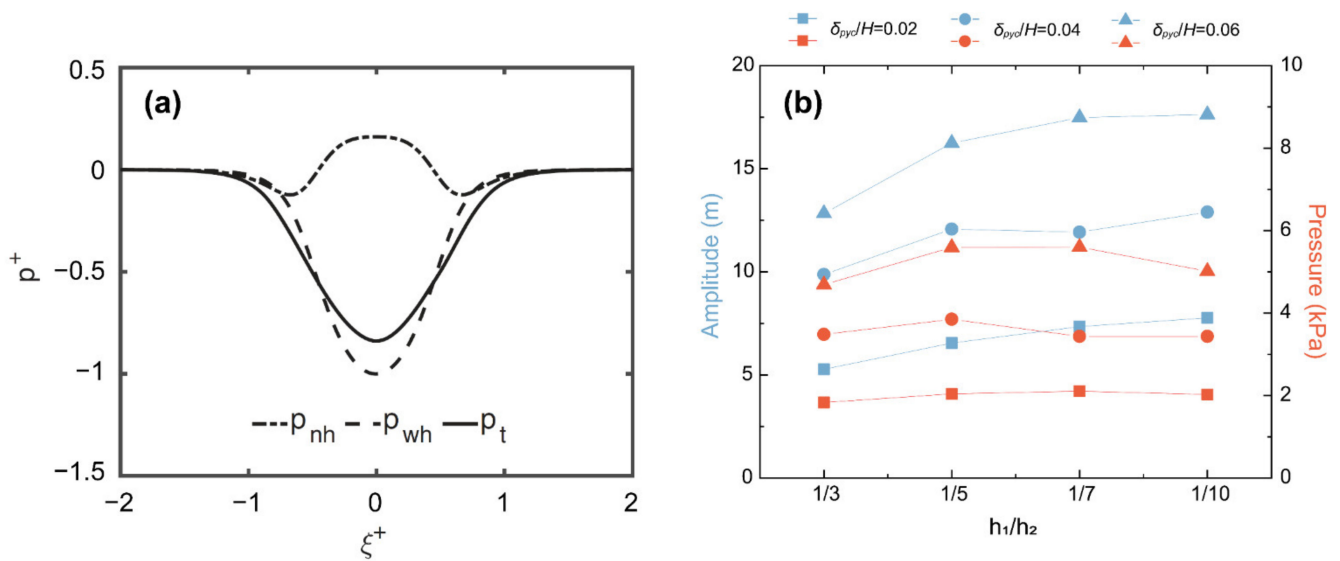


Figure 4. Bottom pressure induced by internal solitary waves for different environmental parameter schemes. (a) ISW-induced bottom pressure with a thickness ratio of $h_1/h_2 = 1/7$. The dash–dash line, dash–dot line, and solid line show the hydrostatic pressure, the non-hydrostatic pressure, and the summation of the above, respectively. (b) Amplitude and pressure changes of ISWs for the different ratios of pycnocline thickness δ_{pyc} and the ratio of upper and lower water depths. Panel (a) adapted from Rivera-Rosario et al. [21], with permission from Wiley. And the data of panel (b) come from Table 2 of Rivera-Rosario et al. [21].

2.2. Observation Results

Published observations of pressure disturbance by NLIWs provide the most realistic seabed response, which can be compared with the numerical results to examine the pressure model. The in situ NLIW pressure results from each of the observation regions are reviewed below (as shown in Table 1).

Table 1. Summary of past 15 years on the observation details of seafloor pressure disturbance induced by internal waves.

Observation Area	Range	Water Depth (m)	Transducer	Full Scale (MPa)	Resolution (Pa)	Sampling (Hz)	Height (mab)	Maximum Pressure (kPa)	Wave Event	Wave Amplitude (m)
New Jersey Shelf [43]	38.80–39.2° N 72.75–73.50° W	70–110	Paroscientific Model 6000-200A	1.4	1.4	1	0	−0.765	Depression NLIWs	/
Massachusetts Bay [11]	41.78–42.68° N 69.99–71.09° W	10–80	Paroscientific Model 6000-200A	1.4	1.4	1/0.5	0	±0.2	High-frequency NLIWs	~20

Table 1. Cont.

Observation Area	Range	Water Depth (m)	Transducer	Full Scale (MPa)	Resolution (Pa)	Sampling (Hz)	Height (mab)	Maximum Pressure (kPa)	Wave Event	Wave Amplitude (m)
Great Meteor Seamount [53]	30.00° N 28.30° W	549	Sea-Bird Scientific SBE 53	/	/	0.33	1.7	0.05	High-frequency internal waves	/
Marsdiep Strait [20]	52.98° N 4.77° E	23	Sea-Bird Scientific SBE 26	/	/	4	0.08	0.1	High-frequency internal waves	/
South China Sea [19]	20.3° N 115.4° E	481	/	/	/	/	10	20	Obliquely incident ISWs	~80
South China Sea [54]	/	/	/	/	/	/	/	4	Depression ISWs	/
Aogashima Island Slope [55]	32–33° N 140–141° E	1470–2240	Paroscientific 8B7000-I-005	68.95	/	4/0.7	0	0.05	Internal tide wave	/

Note: mab—meters above the bottom; SBE—Sea-Bird Electronics; NLIW—nonlinear internal waves; ISW—internal solitary waves.

2.2.1. North American Atlantic Coast

In the Shallow Water 2006 experiment on the New Jersey shelf, Moum and Nash [43] deployed three Paroscientific Model 6000-200A pressure transducers (sampled at 1 Hz) mounted in three landers, respectively, to capture NLIWs that propagate onto the shelf. These seafloor NLIW pressure measurements provide adequate experimental verification to confirm the NLIW pressure model derived by Moum and Smyth [46]. Furthermore, observed NLIW trains supply a detailed understanding of the NLIW pressure field which has not previously been quantified. The seafloor NLIW pressure disturbance signals become visible by a low-pass bandpass filter at 1/20 Hz and a high-pass bandpass filter at 1/2000 Hz. A train of negative bottom pressure signal relates to the typical signatures of horizontal and vertical components of NLIWs velocity and the maximum pressure magnitude over 765 Pa (as shown in Figure 5). In addition, it does not appear that NLIW packets have a powerful pressure signal and near seabed current velocity [43].

Most importantly, the correlation between pressure and velocity provided an important understanding of the spatial distribution and structure of NLIW energy transport flux [7,11]. Thirteen high-frequency NLIW packets were observed within 6.5 days in Massachusetts Bay [11], with obvious pressure properties in along-shore and cross-shore spatial variability. The bottom pressure data were collected from an array of 14 Paroscientific Model 6000-200A pressure transducers at 1 Hz or 2 Hz and band-pass filtered low-pass at 1/120 Hz and high-pass at 1/1800 Hz to distinguish the NLIW pressure signal. The pressure amplitude oscillations weaken from 580 Pa to 36 Pa with NLIW propagation cross-shore to the shallow sea (as shown in Figure 6), accompanied by synchronized decay of the high-frequency NLIW energy. Thomas et al. [11] argued that the strong connection between kinetic energy and seabed pressure variation allows qualitatively the kinetic energy variability of high-frequency NLIWs using the bottom pressure transducer array. Moreover, because of the strong dependence on background shear currents and water depth, an attempt to quantify the NLIW energy flux is impracticable.

Because of the significant seafloor pressure response by NLIWs, the ocean bottom pressure (OBP) direct measurement allows real-time automated detection and alert of NLIWs [12,55] without on-duty personnel or expensive instrumentation. Stöber and Moum [12] demonstrate an NLIW detection algorithm using seafloor pressure data from the New Jersey shelf, which could be employed for warning wave events that pressure amplitude over 250 Pa. Before this, OBP was commonly used for the detection of tsunamis [56], seismic waves [57], seafloor deformation [58], and many others.

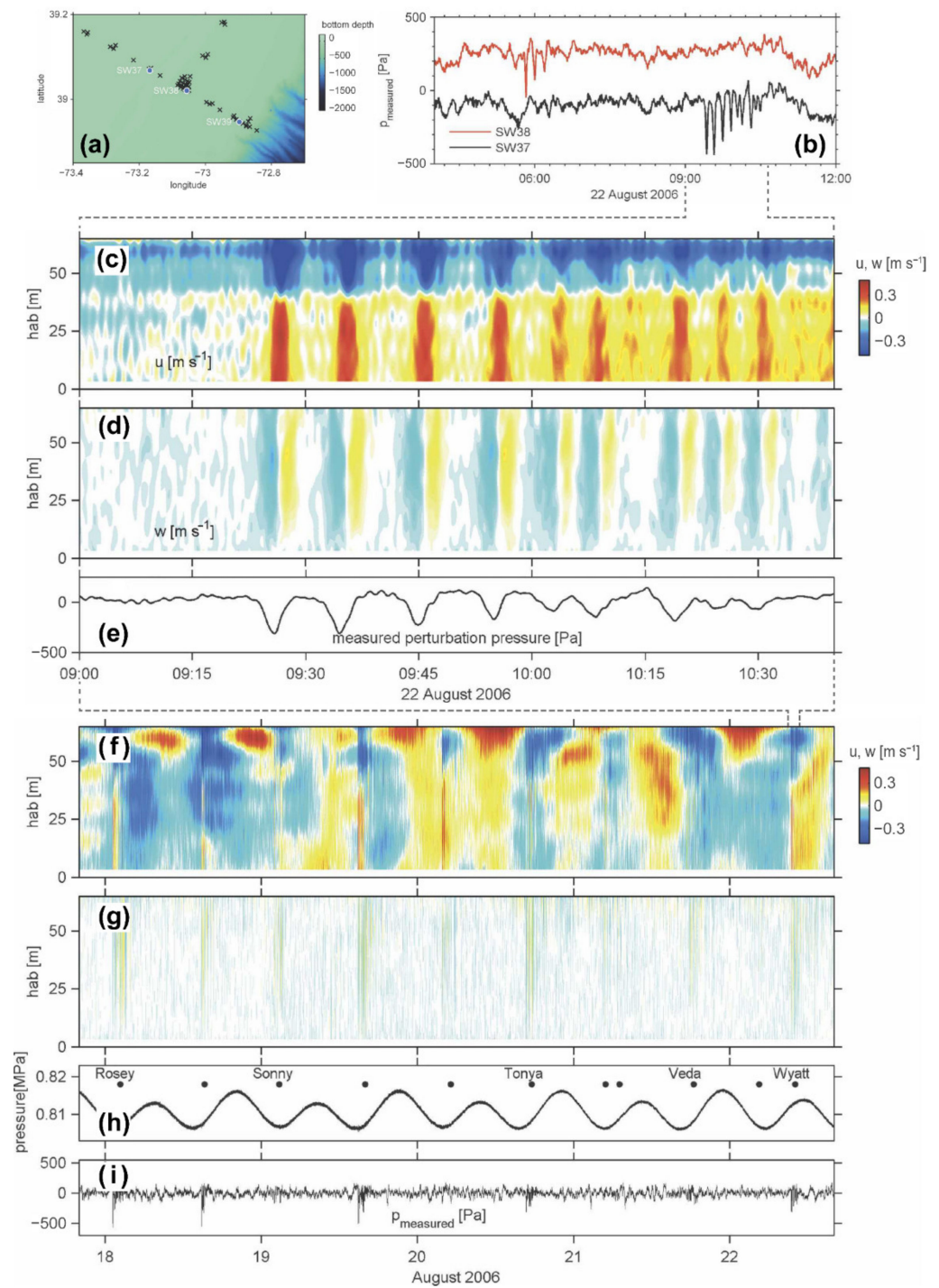


Figure 5. Seafloor pressure measurements of NLIWs on the New Jersey shelf. (a) Mooring locations of SW37, SW38, and SW39 where bottom pressure observations were conducted. (b) The NLIW named Wyatt induces bottom pressures at SW37 and SW38, respectively. Note the bottom pressure signals have been offset for clarity. For NLIW Wyatt, comparison between horizontal velocity (c), vertical velocity (d), and bottom pressure (e) at SW37 on 22 August 2006. For all NLIW observed at SW37, comparison between time series of (f) horizontal velocity, (g) vertical velocity, (h) bottom pressure, and (i) filtered bottom pressure from 18 to 23 of August 2006. Dots in (h) show the named NLIWs, including NLIW Wyatt. The hab is expressed as height above the bottom. Panels (a–i) adapted from Moum and Nash [43], with permission from the American Meteorological Society.

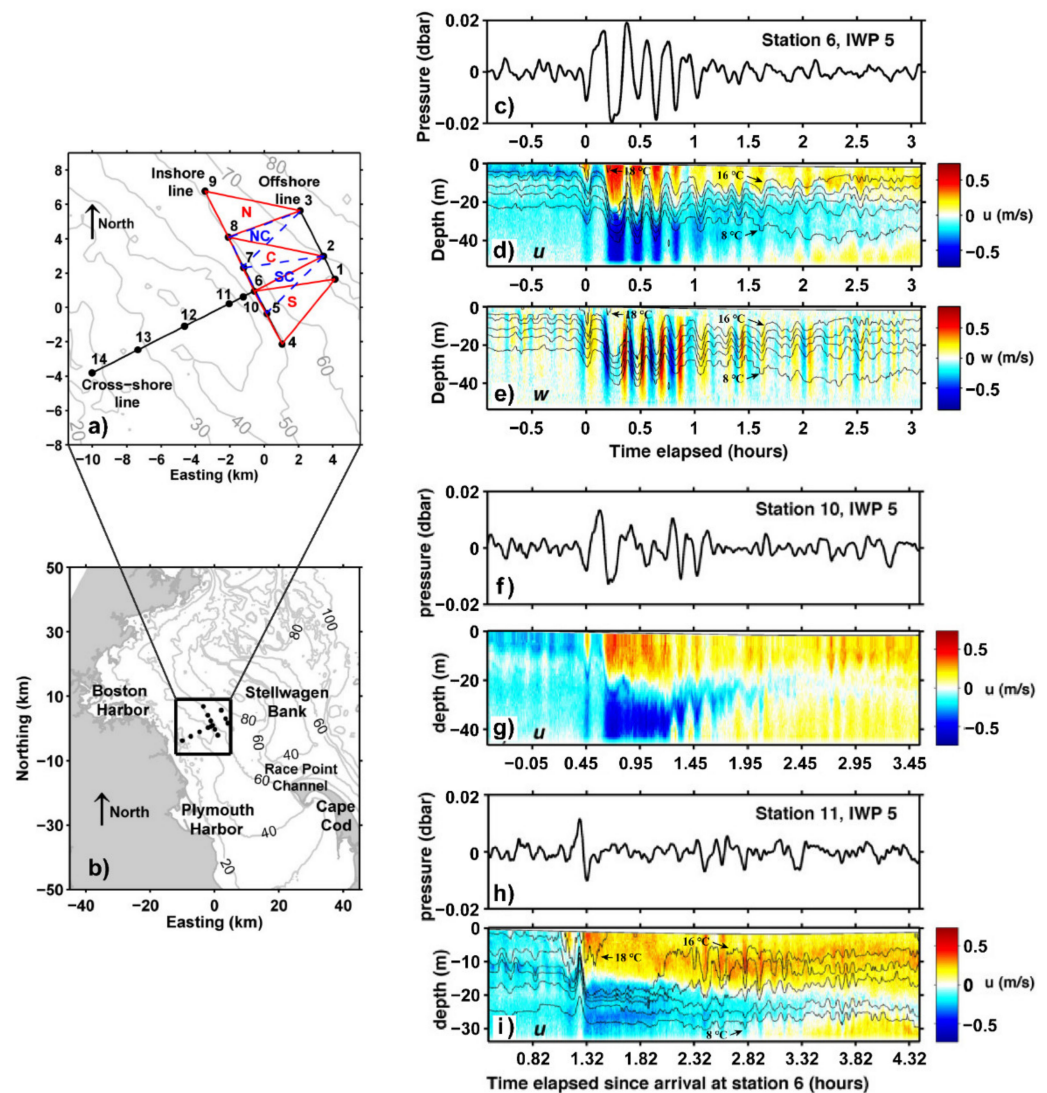


Figure 6. Seafloor pressure variability of the internal wave packet (IWP) in Massachusetts Bay detected by a sensor array. (a) Station locations (black dots) of bottom pressure sensors. (b) Map of the investigation area in Massachusetts Bay, the black box is (a). For IWP 5, comparison between (c) filtered bottom pressure, (d) horizontal velocity u and temperature, and (e) vertical velocity w and temperature at station 6. Comparison between (f) filtered bottom pressure and (g) horizontal velocity u at station 10. Comparison between (h) filtered bottom pressure and (i) horizontal velocity u and temperature at station 11. The temperatures in (d,e,i) represent black contour lines at 2 °C intervals from 8 °C to 18 °C. Time 0 h is the timing of IWP 5 reaching station 6. Panels (a–i) adapted from Thomas et al. [11], with permission from Wiley.

2.2.2. North American Pacific Coast

In the Oregon shelf, the properties of ISWs, internal bores, and gravity currents were observed concurrently with high-intensity acoustic scattering layers induced by sediments resuspending having a vertical extent over 30 m above the seafloor [7]. A SeaBird conductivity and temperature recorder that was located 1 m above the bottom captured intense pressure pulses due to NLIW propagation. Mowm et al. [7] found that the pressure–velocity energy flux had significant contributions from the effects of non-hydrostatic and free surface displacement, which implied the substantial impact of non-hydrostatic pressure and external hydrostatic pressure perturbation. The vertical component of non-hydrostatic effects and free surface displacement dominates the NLIW energy transporting near the seabed.

2.2.3. South China Sea

Energetic ISWs were consistently observed in the South China Sea, causing strong near-seabed oscillatory currents over 0.8 m/s [19]. A pressure dramatic fluctuation has been found over 2 kPa using a pressure transducer mounted on a mooring at about 10 m above the seabed, which was accompanied by an ISW with an amplitude exceeding 80 m crossing the slope (as shown in Figure 7). The largest velocity of the westward and northward components are both over 0.4 m/s. Yang et al. [54] observed large amplitude depression ISWs of mode-1 with large amplitude produced near bottom pressure perturbations more than 4 kPa in the South China Sea. A 2.5 kPa bottom pressure event is induced by ISWs, which corresponds to approximately 1.5 m/s velocities in the horizontal component. The bottom pressure perturbation caused by ISWs can be described well by the Bernoulli balance.

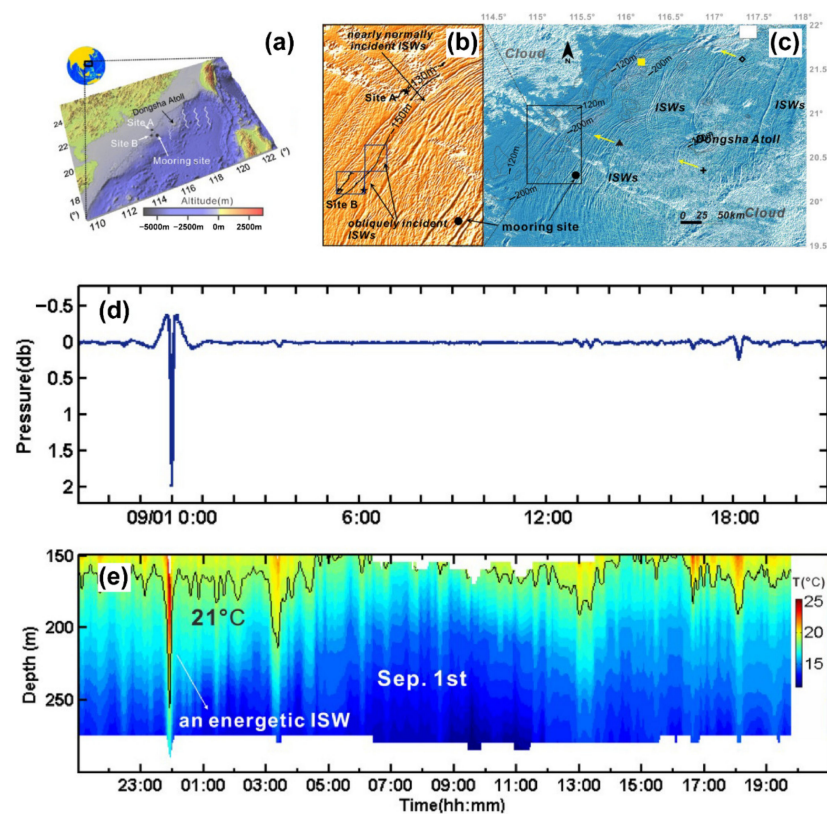


Figure 7. Seafloor pressure of obliquely incident ISWs in the northern South China Sea. (a) Location of the mooring site. (b) Expansion of boxed region in (c). The obliquely incident ISWs (deep brown imprints) near the mooring site are shown in the amplified MODIS image. (c) The MODIS image illustrates the ISWs’ direction. Approximately 2.5 kPa of pressure changes at 10 m above the bottom at the mooring site (d), when the largest fluctuation of 21 °C isotherms is down about 80 m (e), reflecting a crossing energetic ISW propagation. Panels (a–e) adapted from Ma et al. [19], with permission from Wiley.

2.2.4. European North Atlantic Coast

In the Marsdiep strait between Texel Island and the Netherlands mainland, van Haren [20] observed a pressure oscillation corresponding to high-frequency internal wave propagation using a SeaBird SBE 26 wave and tide recorder with a pressure transducer (4 Hz sampling rate). The spectra analysis of bottom pressure was used to distinguish the surface waves, near-surface turbulence and waves by wind and ferry, turbulent overturns, and high-frequency internal waves. van Haren [59] synthesized bottom pressure data collected in the range from a shallow Marsdiep strait via the Baltic Sea and the seamount in the open Atlantic Ocean to the deep Gulf of Mexico and assessed contributions of internal waves and turbulence in different bottom pressure data with the support of additional temperature and current data. All observations are in sloping bottom topography, where

NLIW propagation becomes near critical and shows internal wave–turbulence transition. In the Great Meteor Seamount of the Atlantic Ocean, van Haren [53] observed that the pressure changes were equivalent to the fluctuation of hydrostatic pressure due to high-frequency internal waves propagating up to 100 m above the bottom and non-hydrostatic pressure (reduced by 50 Pa) following turbulence due to breaking of the internal wave in the range of 50 m above the bottom.

2.2.5. Japan Western Pacific Coast

On the eastern slope of Aogashima Island, Fukao et al. [55] observed the power spectral density of the pressure changes of the M2 internal tide, using a pressure transducer array of 10 stations with a 10 km distance that formed equilateral triangles. The results show that the pressure power spectral density of the M2 internal tide was about $10^8 \text{ Pa}^2/\text{Hz}$, equivalent to a bottom pressure on the order of 50 Pa.

3. The Pore-Pressure Variation of the Seabed

The pore-pressure variation of the seabed occupies a central position in seabed dynamic responses during the NLIW-action for conceptual and practical reasons. Conceptually, pore pressures are necessary to evaluate seabed seepage from calculated vertical gradients and thus to allow the rational explanation of the sediment resuspension and benthic boundary layer instability. Previously, from a theoretical perspective, sediment resuspension caused by internal waves was recognized as an issue with hydrodynamic stability [2]. Practically, the pore pressure in marine sediments is often an easier measure than other aspects of seabed-response behavior, because it is omnidirectional [60]. At present, there are theoretical and numerical results in the study of pore-pressure variation by NLIWs. The following subsections set forth the basic theoretical formulations and characteristics of pore-pressure response and some of the experimental evidence for their existence.

3.1. Governing Equations for Pore-Pressure Response

The fundamental theory for porous seabed response was first developed in surface waves and further considered in internal waves by Chen and Hsu [23]. Biot’s consolidation equation has been widely used for wave–seabed interactions since 1978 [32] and was discussed in depth in Jeng [61,62]. The description of the seabed is, in general, based on the equations of compressible fluids in an elastic and infinite-thickness porous media. The fluid flow in the pore space of the porous seabed obeys Darcy’s law.

Using a combined model of Biot’s consolidation equation in the two-dimensional space [63] and the storage equation [64], Chen and Hsu [23] presented a numerical method for the pore pressure and sediment displacements in an isotropic poroelastic seabed induced by internal waves. The governing equation of excess pore pressure P in the seabed is written as

$$K_x \frac{\partial^2 P}{\partial x^2} + K_z \frac{\partial^2 P}{\partial z^2} - r_w n \beta \frac{\partial P}{\partial t} = r_w \frac{\partial \varepsilon}{\partial t}, \tag{11}$$

where K_x and K_z are the permeability coefficients in the x and z directions, respectively, r_w is the unit weight of the pore water in the seabed, n is the porosity of sediment, and β is the compressibility of the pore fluid in the seabed. The ε is the volume strain obtained by

$$\varepsilon = \frac{\partial \xi}{\partial x} + \frac{\partial \chi}{\partial z}, \tag{12}$$

where ξ and χ are the sediment displacements in the x and z directions, respectively. Moreover, further consideration of the parameterization of saturation S_r , the compressibility β is given by

$$\beta = \frac{1}{k_w} + \frac{1 - S_r}{P_0}, \tag{13}$$

where k_w is the bulk modulus of elasticity of water and P_0 is the absolute pore pressure. The excess pore pressure P , volume strain ε , and sediment displacements that ζ and χ can be related by equilibrium equations that are written as

$$G\nabla^2\zeta + \frac{G}{(1-2\mu)} \frac{\partial\varepsilon}{\partial x} = \frac{\partial P}{\partial x}, \tag{14}$$

$$G\nabla^2\chi + \frac{G}{(1-2\mu)} \frac{\partial\varepsilon}{\partial z} = \frac{\partial P}{\partial z}, \tag{15}$$

where μ is the Poisson ratio and G is the shear modulus and can be related by

$$G = \frac{E}{2(1+\mu)}, \tag{16}$$

where E is the Young modulus. The governing Equations (11)–(16) incorporated within the boundary conditions constitute the components needed from which the pore pressure and sediment displacements in the seabed can be solved [23]. On the basis of Biot’s consolidation equation, the seabed response theories proposed by Chen and Hsu [23] have been used widely with some success to model the seabed interaction with internal waves [35,47,65].

Pore-pressure response inside the porous seabed has been explored with numerical solutions of the mass conservation equation [66]. More recent examples are the numerical examining of Rivera-Rosario et al. [21], who sought solutions for a pore-pressure response for large-amplitude NLIWs. In this method, the seabed horizontal deformation was neglected. The pore pressure p is expressed as

$$\frac{k}{\rho_0 g} \nabla^2 p = (\alpha(z) + n\beta) \frac{\partial p}{\partial t}, \tag{17}$$

$$\alpha(z) = \frac{1}{2\bar{\mu}(z) + \bar{\lambda}(z)}, \tag{18}$$

where k is the permeability of the seabed, ρ_0 is the reference density of the seawater, $\alpha(z)$ is the vertical compressibility, n is the porosity, β is the compressibility and is determined by Equation (13), $\bar{\mu}$ is the effective shear modulus, and $\bar{\lambda}$ is Lamé’s effective first parameter. The numerical method of Fourier–Legendre collocation is used to solve Equation (17).

Although the seabed is an elastoplastic material, the elastic models have played the primary role in elucidating the transient features of the pore pressure and deformation, if not considering the precise details of permanent deformation and accumulated pore pressures. They have the advantage of permitting modeling with reduced equations wherein the parameters are fewer and easy to obtain. For elastoplastic models, accumulated pore pressures and deformation can be studied, but the ease of generalization is often lost. Furthermore, internal waves are restricted to slower phase velocity and longer periods compared with surface waves and were consequently considered unable to generate pore-pressure build-up. Thus, the elastic models have been adopted as the wide application of choice. However, elastoplastic models are needed to accurately describe the properties of seabed dynamic responses.

3.2. Vertical Profile of the Pore-Pressure Changes

The changes in internal waves inducing pore pressure of the transient state were considered firstly by Chen and Hsu [23] and the instance of NLIWs is further considered by Rivera-Rosario et al. [23]. Along with the propagation of depression NLIWs, a negative pore-pressure enhancement occurred inside the superficial seabed under the trough of the wave [23,35], when a strong countercurrent against the wave direction was present as positive pressure imposed from the bottom boundary layer down into the seafloor [43,46]. Since the total pressure load by NLIWs is negative, the wave propagation produces an

insufficiency in the pre-existent pore pressure and this insufficiency is more obvious under the wave trough [21]. Before the arrival of the wave trough, the pore pressure inside the superficial seabed shows a slight increase, roughly estimates one order of magnitude lower than that under the wave trough, and decays rapidly in the deeper seabed (as shown in Figure 8). This is corresponding to the horizontal pattern of the bottom pressure disturbance by NLIWs.

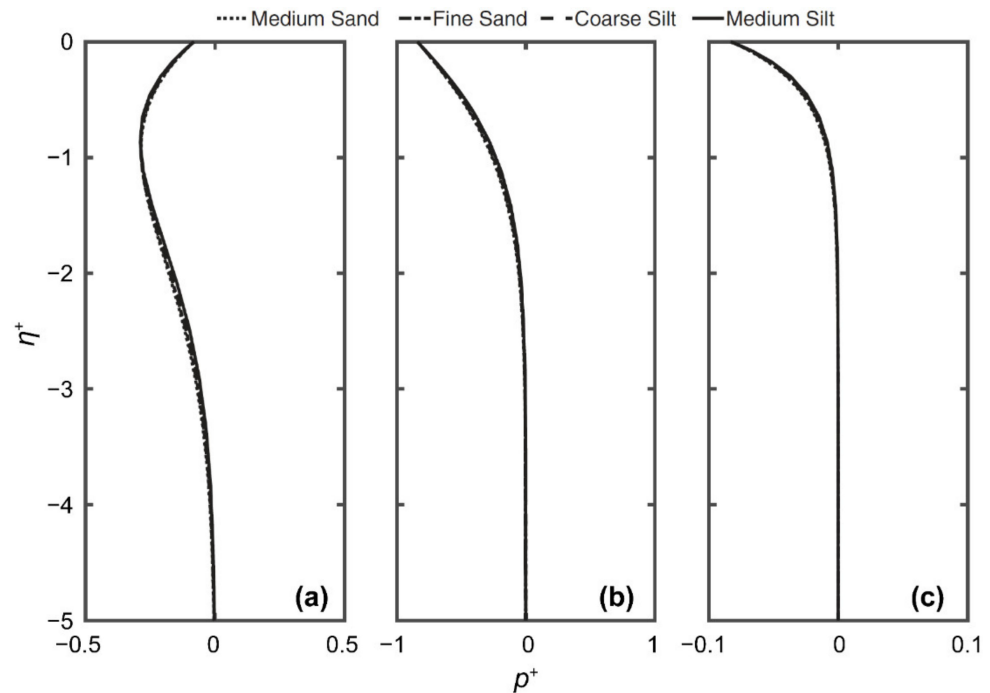


Figure 8. Pore-pressure changes in the vertical direction by ISWs. For different seabed materials, the changes of pore pressure, where (a) is after the ISW trough, (b) is under the ISW trough, and (c) is before the ISW trough. Panels (a–c) adapted from Rivera-Rosario et al. [21], with permission from Wiley.

After the passage of the wave trough, the superficial pore pressure is attenuated to the degree before the wave trough, but the pore-pressure insufficiency persists under the seafloor after the wave has passed by. Rivera-Rosario et al. [21] employed an effective diffusion coefficient κ based on Equation (17) to simulate the phenomenon of pore-pressure lag. This phenomenon of lag was first observed in surface wave induced pore-pressure response [32]. The effective diffusion coefficient κ is expressed as

$$\kappa = \frac{k}{\rho_0 g (\alpha(z) + n\beta)} \tag{19}$$

with units of length squared over time. Since the pressure diffusive time scale, L_w^2/κ , is larger than the time scale of the ISW propagation, L_w/c , a pore-pressure phase lag inside the seabed will occur after the passage of the wave trough (as shown in Figure 8).

The numerical results depicted that vertical distributions of the negative pore-pressure by internal waves decrease as the soil depth increases, but the rate of pore-pressure decay depends on the wave and seabed parameters [22,23]. A parametric method is applied to examine seabed dynamic responses induced by NLIWs and has been considered in detail in numerous studies [22,23,47]. Chen and Hsu [23] compared vertical pore-pressure decay by varying relevant parameters of internal wave characteristics and seabed properties. The results demonstrate that the rate of pore-pressure decay occurs faster when accompanied by a large water depth and an internal wave period, as well as the sediment permeability and saturation, or small sediment shear modulus, hydraulic anisotropy, and porosity.

High-accuracy numerical simulations on the NLIWs with large amplitude reported the variations in pore pressure to penetrate deeper into the seabed by a depression wave in the presence of a small amount of pore gas in the seabed [21]. The content of trapped-pore-gas increase will strengthen the pore-pressure build-up and provide steeper vertical gradients in the seabed. For a high permeability of sediment, the negative pore pressure will penetrate deeper into the seabed and approaches a length comparable to the amplitude of ISWs [21], but also means that the pore pressure will dissipate faster compared with low permeability of sediment. For NLIWs in a lake environment, Olsthoorn et al. [22] demonstrated that the long wavelength induced the penetration depth of pore-pressure increase and expanded the range of seepage through the porous domain. Tian et al. [35] modeled seabed pore pressure and experimentally visualized pore-pressure penetration depth from ISWs over a sloping bottom. The results presented that the perturbations approximated tens-to-hundreds of meters in extent, one order of magnitude smaller than the wavelength, which perhaps was deeper than that of surface wave induced pore-pressure changes. Nevertheless, in other studies, the quantification of penetration depth from ISWs was not as clear. Rivera-Rosario et al. [21] found the depth in a pore-pressure impact approximately 1 m below the water-sediment interface, for a seabed with lower permeability. They argued that the higher phase velocity of NLIWs implies an enhancement of the pore-pressure build-up near the superficial sediments but will not permit deeper in the seabed (Figure 9).

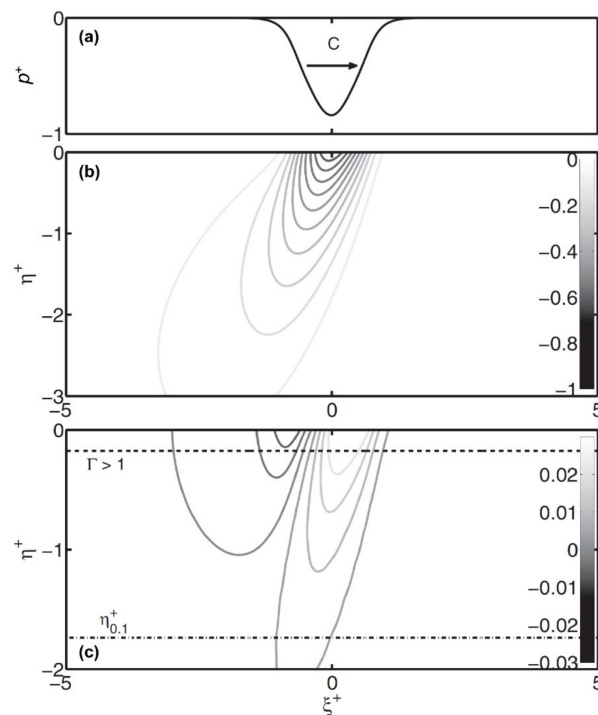


Figure 9. Contour of the pore-pressure changes by ISWs. The ISW traveling to the right with phase speed c , where (a) is the ISW-induced pressure forcing and (b) is the pore-pressure changes for an unsaturated seabed composed of medium sand. (c) Vertical pore-pressure gradient with an unsaturation seabed composed of medium silt. The dashed-dot line marked as $\eta_{0.1}^+$ shows the penetration depth, where the changes of pore pressure are 10% of the bottom pressure under the wave trough. The dashed line marked as $\Gamma > 1$ shows the failure criterion, where the buoyant unit weight of sediment is less than the vertical pore-pressure gradient. Panels (a–c) adapted from Rivera-Rosario et al. [21], with permission from Wiley.

The experimental investigation of Tian et al. [35] provided qualitative confirmation of the theoretical predictions of the pore-pressure changes caused by NLIWs. The experiments were conducted with a 9° slope and the negative pore-pressure inversion accompanied by depression ISW shoaled and transformed into an elevation wave was observed. In the

experimental work by Qiao et al. [67], a similar negative pore-pressure depression was observed along with sediment resuspension during the ISW breaking as the depression wave shoaled, indicating that the seabed response is sufficient to produce a significant contribution to sediment resuspension. The phenomenon of polarity changes and the breaking of ISW has been observed in continental slopes [68–70]. Li et al. [71] experimentally visualized the pore-pressure response from ISWs over a sloping bottom. The results demonstrated that the accumulation and release of pore pressure occurred simultaneously before the seabed failure, but the increase of the wave amplitude will enhance the release process. Although experiments may guide first-order pore-pressure dynamic responses by NLIWs, direct application to the in situ observation must be conducted with circumspection.

3.3. Potential Failure Due to Seabed Instability

The above review motivates further consideration of potential failure due to seabed instability under the presence of pore-pressure changes by NLIWs. The motivation is to emphasize the contribution of the seabed dynamic response induced by NLIWs during seabed instability and to motivate subsequent in situ measurements that will support the theoretical findings. The transient liquefaction of the seabed induced by depression NLIWs was considered by Rivera-Rosario et al. [21]. The vertical pore-pressure gradient can be compared to the buoyant unit weight of sediment as a measure of possible transient liquefaction [66]. The buoyant unit weight γ_s is expressed as

$$\gamma_s = (1 - n)(\rho_s - \rho_0)g, \tag{20}$$

where n is the porosity of the seabed, ρ_s is the sediment density, and ρ_0 is the fluid density in the bottom. Therefore, if the vertical pore-pressure gradient is greater than the buoyant unit weight of sediment, transient liquefaction will occur, or

$$-\frac{\partial p}{\partial \eta} \geq \gamma_s \tag{21}$$

for a seabed in a fixed reference frame $\xi - \eta$. Thus, yields the normalizing failure criteria Γ of transient liquefaction by NLIWs as

$$\Gamma = \frac{\partial p}{\partial \eta} \left[\frac{(\rho_s - \rho_0)gA}{\gamma_s \eta_0} \right] \geq 1, \tag{22}$$

where A is the amplitude of depression ISW and η_0 is the vertical dimension that is scaled by the diffusive depth as

$$\eta_0 = \sqrt{\frac{\kappa L_w}{c}}, \tag{23}$$

where κ is the effective diffusion coefficient, L_w and c are the half-wavelength and phase speed of depression ISW, respectively. With the early exploration of the fully nonlinear model of NLIWs with numerical solutions of the DJL equation, Rivera-Rosario et al. [21] recognized that the pore-pressure changes influence roughly the top 1 m of the thickness of the low-permeable seabed, with only 2 cm sediments appearing in transient liquefaction under the superficial seabed. When the saturation of the seabed is decreased, the vertical pore-pressure gradient is powerful enough to exceed the buoyant unit weight and induce sediment transient liquefaction observed in the simulation [21]. In the experimental work by Li et al. [71], elevated pore-pressure response with a decreased gradient of the slope was seen as the ISW shoaled during the drawdown period before breaking, indicating that the gently sloped seabed response is more sensitive to the wave amplitude changes.

For the stratified water column, the elevation NLIWs can form when the thickness of the upper layer is larger than that of the lower layer [69,72,73]. The mechanisms of seabed failure induced by the elevation NLIWs were argued by Rivera-Rosario et al. [21]. Due to the positive bottom pressure load dominated by hydrostatic pressure [46], related to the

pycnocline displacement, positive pore pressure penetrated the seabed as a result of the elevation NLIWs. The vertical pore-pressure gradient was also generated by the elevation NLIWs, but was insufficient to exceed the buoyant unit weight of the sediment [21]. Thus, during the propagation of elevation NLIWs, the wavefront is steep enough to induce a horizontal pore-pressure gradient that is powerful enough to overcome the mobilized internal friction of the seabed and capable of resulting in seabed failure [74]. Based on Equation (17), for a seabed in a fixed reference frame $\zeta - \eta$, the dimensional seabed failure criterion can be expressed as

$$\frac{\partial p}{\partial \zeta} > \gamma_s \tan \phi, \tag{24}$$

where ϕ is the angle of internal friction ϕ of the seabed. Equation (24) has been used to examine seabed instability by a surface solitary wave [75].

While there is no in situ measurement of the pore-pressure changes for NLIWs, field observation, including surface wave-induced seabed failure, has reported referable results. Torum [76] reported that pore-pressure changes induced by surface waves penetrated more than 10 m depths in the unsaturated seabed. Another fieldwork by Cross et al. [77], reported pore pressure reaching 37 m below the seafloor by a surface wave height of at least 3 m at a water depth of 5 m. Bennett and Faris [78] found a penetration depth of more than 6 m at the Mississippi Delta at a water depth of 13 m. However, as noted earlier, a similar study implies that the depth below the seafloor of NLIWs inducing seabed instability would be smaller than that of surface waves, but has not been explored in a detailed examination with strong NLIWs in the field.

4. The Seepage and Fluid Circulation in Sediment

The vertical gradient of pore pressure within the seabed can be a measure of seepage in the vertical direction and, therefore, of the possible impact on sediment resuspension [21]. Seepage of pore fluid in a permeable seabed was accompanied by fluid circulation through the sediment–water interface [22], which can have far-reaching implications on heat and chemical exchanges between the seabed and the water column [45,79]. The primary manner of generating seepage and fluid circulation in sediment is through the spatial variability of pressure fluctuations at the bottom [80]. In recent years, few studies have examined the seepage and fluid circulation induced by the passage of an NLIW in any systematized way; rare numerical results in existence are presented below.

4.1. Governing Equations for Seepage of Pore Fluid

Darcy’s law is a classical relationship that links pore-pressure gradients and the seepage velocity in the seabed, although it is experimentally determined. Once the wave pressure distribution is determined at the bottom, the distribution of fluid seepage in the seabed can be acquired by Darcy’s law [81]. A useful extension of the fluid seepage due to internal waves was proposed by Olsthoorn et al. [22]. They calculated that NLIWs caused seepage through the lakebeds of deep regions, where surface gravity waves had little impact, using the Dubreil-Jacotin–Long (DJL) equation and Darcy’s law. The lakebed is assumed to be rigid and saturated, thus the seepage velocity \vec{w} based on Darcy’s law is expressed as

$$\vec{w} = -\frac{k}{\mu} \nabla (P + \Pi), \tag{25}$$

where k is the permeability of the lakebed, μ is the dynamic viscosity which is assumed to be a constant for a given fluid, P is the pressure, and Π is the gravitational potential energy per unit volume. $P + \Pi$ in Equation (25) is defined as the gauge pressure. For an incompressible fluid, the condition is expressed as

$$-\nabla \cdot \left(\frac{k}{\mu} \nabla P \right) = 0. \tag{26}$$

Furthermore, the stratification of permeability k in the porous lakebed was considered and was taken as a hyperbolic tangent function. The permeability k is written as

$$k_{Inc} = 1 + \frac{1}{2} \left[1 + \tanh \left(\frac{z - 0.5}{0.1} \right) \right], \quad (27)$$

$$k_{Dec} = 2 - \frac{1}{2} \left[1 + \tanh \left(\frac{z - 0.5}{0.1} \right) \right], \quad (28)$$

where k_{Inc} and k_{Dec} are the permeability k for increasing and decreasing in the vertical direction of the seabed, respectively.

The impressive point of the seepage model presented above was to employ the bottom pressure extracted from the solution of the DJL equation to drive seepage in a porous lakebed. However, this model has a potential limitation as a seepage tool by NLIWs. As opposed to previous numerical results [21,35], the seepage model proposed by Olsthoorn et al. [22] showed that the seepage velocity magnitude distributions are symmetrical across the crest of NLIWs (Figure 9). Rivera-Rosario et al. [21] found that the seepage is asymmetrical about the wave trough since the bottom pressure of NLIWs translates along the seabed. Thus, the NLIWs leave a diffusive imprint of pore pressure during their passage, which is similar to that described under surface solitary waves [75].

4.2. Seepage Variations Due to Internal Wave Propagation

During internal wave passage, the seepage of pore fluid variations inside the porous seabed have been explored with numerical solutions of the DJL equation. More recent instances are the research of Olsthoorn et al. [22] and Rivera-Rosario et al. [21], who sought seabed solutions for seepage and potential failure, respectively. Olsthoorn et al. [22] investigated the seepage field due to wind-generated internal waves in the lake and found the geometrical field of seepage is powerfully governed by both the topography and the ratio of seabed thickness to the bottom pressure broad (Figure 10). The numerical results show that the depression NLIWs act essentially as a vacuum cleaner because of their intrinsic negative bottom pressure to extract the pore fluid from the seabed. For depression NLIWs, the pore fluid is drawn out under the wave trough where negative pressure is highest and invades in the seabed regions along the wave flanks where negative pressure vanishes. A similar phenomenon was previously found by Huettel et al. [82] in the laboratory context. They demonstrated that the traced particles suspended in the bottom boundary layer intruded quickly into the upper layer of sandy sediments, driven by interfacial flows related to topography. Simultaneously, the increased bottom pressure at the upstream and downstream of a small dune drove water access to the interior and the decreased bottom pressure downstream of the slope drew pore fluid from the interior to the water column.

In a numerical study of the generation of seepage in the porous seabed driven by trapped internal waves, Olsthoorn et al. [22] showed the evolution of the vorticity due to trapped internal waves inducing the currents, which indicates the expansion of a highly turbulent bottom boundary layer. Smaller particle matter will then be resuspended by the instability bottom boundary layer and enhanced benthic turbulence, breaking the seal of the surface pores at the seafloor. On the downstream of the trapped internal waves, the consequent permeable changes significantly enhance exchanges between the bottom water and the pore fluid. Rivera-Rosario et al. [21] used the vertical pore-pressure gradient to evaluate the vertical seepage within the seabed. The results demonstrated that the penetration depth of the vertical seepage was significantly sensitive to the seabed permeability and saturation. For an unsaturated seabed with higher permeability, the enhanced negative pore-pressure build-up was accompanied by reduced saturation and penetrated deeper, thus generating steeper vertical pore-pressure gradients, that is, strong vertical seepage within the seabed.

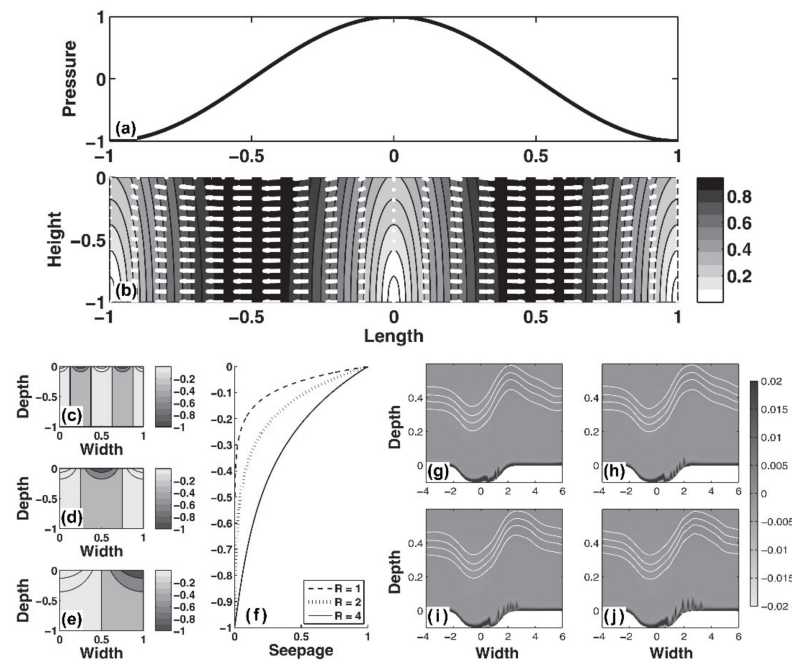


Figure 10. Seepage of pore fluid in lake sediment due to NLIWs propagating. (a) Normalized bottom pressure induced by NLIWs. (b) The contour of the normalized seepage. White arrows indicate the seepage direction. Normalized pore-pressure changes due to sinusoidal pressure forcing for wavelengths (c) $R = 1$, (d) $R = 2$, and (e) $R = 4$. Note the R gives the proportion of the horizontal scale, determined by the bottom pressure perturbation, to the depth of the seabed. (f) The seepage profiles for wavelengths $R = 1$, $R = 2$, and $R = 4$ under the wave trough. Evolution of the normalized vorticity in four nondimensional times of (a) 11.2, (b) 12.6, (c) 14, and (d) 15.4, caused by a development of a highly turbulent boundary layer of the trapped NLIWs. Four white lines expressed as the isopycnic fluctuation of NLIWs. Panels (a–j) adapted from Olsthoorn et al. [22], with permission from Wiley.

4.3. Possible Impact on Sediment Resuspension

As in a previous study, sediment resuspension by NLIWs has traditionally been parameterized according to the bottom shear stress or Shields parameter [2]. High bottom shear stress induced by NLIWs, which may trigger sediment movement sufficiently, resuspended sediments by bottom boundary layer instability [7,83–85]. Nevertheless, in some studies, the results indicated that resuspension events occurred in durations of low bottom shear stress [83,86,87], which indicated a vague relationship between sediment resuspension and bottom shear stress (Figure 11). It is confirmed by oceanic observations that only reaching a critical bottom shear stress does not sufficiently lead to sediment resuspension [83], and that enhanced vertical fluid motions that boost sediments off the seabed are required [88,89].

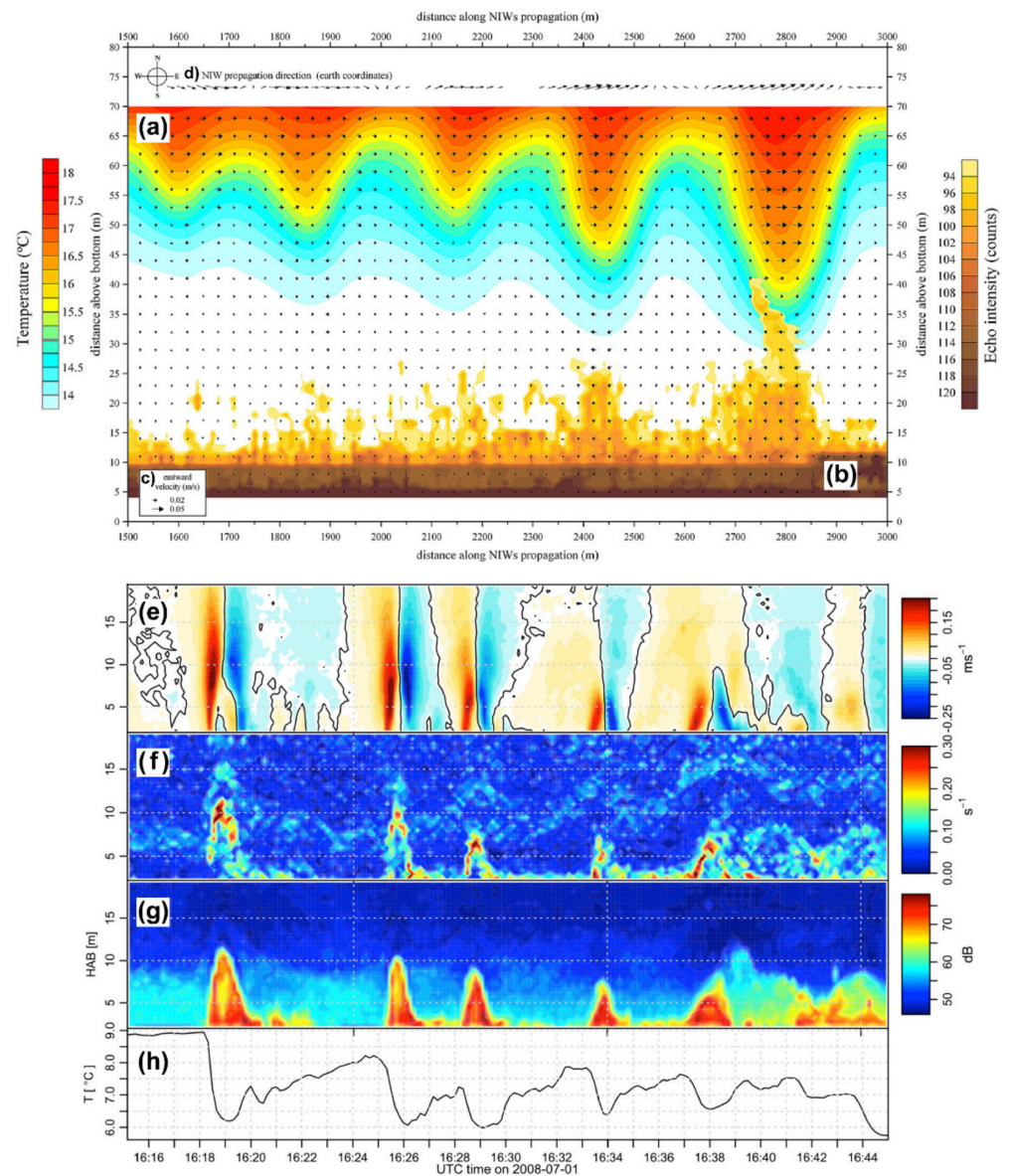


Figure 11. Sediment resuspension due to NLIWs propagating. Comparison between (a) temperature profile, (b) echo intensity, (c) eastward velocity, and (d) NLIW propagation direction during an NLIW train propagation. A 30 min segment of an NLIW shoaling event, comparison between (e) vertical velocity, (f) vertical shear of the horizontal current, (g) acoustic backscatter, and (h) bottom temperature. The black line in (e) shows zero. Panels (a–d) adapted from Quaresma et al. [84], with permission from Elsevier, and panels (e–h) adapted from Richards et al. [90], with permission from Wiley.

The known mechanisms leading to sediment resuspension by NLIWs discussed above fall into the problem of hydrodynamic stability. Aghsaee et al. [91] parameterized sediment resuspension to the Shields parameter θ_{ISW} , which is written as

$$\theta_{ISW} = \frac{\tau_{ISW}}{(\rho_s - \rho_0)gd'} \tag{29}$$

where τ_{ISW} is the shear stress in the bottom, ρ_s is the sediment density, ρ_0 is the fluid density in the bottom, and d is the particle size. However, for the particle incipient motion, the vertical seepage in the seabed was an additional force to be reckoned with since it works to reduce the buoyant weight of the sediments, thus easily inducing suspension. Therefore, Chen and Hsu [23] revisited the issue using a linear internal wave model; the soil

response was solved by the equation equilibrium and the storage equation. The numerical results show that the maximum sediment displacements on the seafloor are 38 m in the horizontal direction and 15 m in the vertical direction. Although it is widely known that the internal waves for large amplitude described by the linear wave model are inaccurate, the mechanism of sediment resuspension considered as the soil displacements induced by internal waves [23] is believed to hold. In addition, Rivera-Rosario et al. [21] considered the vertical seepage force and derived a modified Shields parameter to address the problem of particle incipient motion by NLIWs. For a seabed in a fixed reference frame $\zeta - \eta$, the modified dimensionless Shields parameter θ_{ISW}^+ is written as

$$\theta_{ISW}^+ = \frac{\tau_{ISW}}{(\rho_s - \rho_0)gd - \left[-\partial(p/\gamma_f)/\partial\eta\right]d}, \quad (30)$$

where p is the pore pressure in the bottom and γ_f is the specific weight of fluid. Equation (30) considered NLIW-induced vertical pore-pressure gradient as the vertical seepage force to the modified buoyant force of particles compared with Equation (29). Based on the observation results of Quaresma et al. [84] and the expression of shear stress τ_{ISW} derived by Aghsaei and Boegman [89], the contribution of vertical seepage which represents the magnitude of the reduction in the buoyant weight of the particles is estimated as 11% and 8% for a saturation of 0.97 and 0.99, respectively [21]. Accordingly, the NLIW train will generate an adverse pore-pressure gradient during its passage, performing like a vacuum cleaner to pump out any particles from the seafloor. Thus, this may be a reasonable explanation for the disputed results of powerful resuspension events with low bottom shear stress. Moreover, the NLIW-induced seepage could drive a significant contribution to powerful resuspension events, such as thick nepheloid layers and large subaqueous sand dune formations [24,92].

5. Conclusions and Future Outlook

In general, the seabed dynamic responses induced by NLIWs remain speculative and the guiding theories, models, and experimental data are insufficient. This is coupled with a lack of in situ observation data, especially those that measure both pressure at the seafloor and pore pressure inside the seabed. Consequently, the pressure disturbance and the pore-pressure build-up action as the NLIWs shoal and the interactions with the seabed in continental slope areas remain poorly understood. From large-scale NLIWs (wavelengths of ~ 1 km) to small-scale sediments (particle size of ~ 1 mm), the multiscale process is at fault for the difficulty in investigating the issues [2], which makes in situ observation work challenging. Furthermore, the large Reynolds numbers in the ocean cannot be reproduced in experiments, making a precise simulation experiment of these NLIW–seabed interaction processes a challenge at the laboratory scale [89]. All field-scale numerical simulations of seabed dynamic responses induced by NLIWs do not consider the influence of a permeable seabed on the NLIW evolution and the real-time interactions are not yet resolved in the current models. In actuality, the wavelengths of NLIWs are affected by the permeability of the seabed in addition to the water depth and the wave period [23]. Moreover, the waveform of an NLIW inversion weakens significantly as the seabed porosity increases [93]. Briefly, we lack the numerical method to simulate NLIWs and their interactions with the seabed in multiscale at the necessary field-relevant high resolution.

The vast majority of the NLIW shoaling events appear on gentle slopes [7,68], where the fission of the shoaling wave is the dominant process as the depression NLIW changes to an elevation type and further transforms into a small-amplitude internal wave train during shoaling [94]. However, process studies in field scales on ISW-induced seabed responses have mostly been attempted on flat bottoms [21,23]. In the published literature, the indication of the intricate dynamic response of pore pressure during the transition of NLIW polarity has received little attention. Eventually, the NLIWs arrive at the turning point, where the drawdown of the negative pore pressure and the subsequent accumulation

of positive pore pressure have the potential to induce pore fluid seepage along the slope and further drive potential material exchange across sediment–water interfaces [25,95]. The effect of NLIW-induced seepage boost sediment resuspension is nonnegligible in the slope region [21], but models have still not looked into this effect. Field observations show that the shoaling NLIWs can produce bottom nepheloid layers in horizontal length scales up to hundreds of meters [96] and further spread to the formation of intermediate nepheloid layers in horizontal length scales up to tens of kilometers [24]. In order to parameterize and quantify the potential failure and possible resuspension as a function of pore pressure and boundary slope (of which the latter governs the seabed response mechanism), seabed-related process-based research on continental slopes is necessary [35,67,71].

Our emphasis on the seabed response during the shoaling process of NLIWs is appropriate in view of the in situ observational evidence, but it is also limiting, particularly in deeper water where the pressure forcing of depression NLIWs is generally believed to vanish [43]. Considering the present numerical and experimental difficulties associated with the examination of seabed dynamic responses induced by NLIWs, there is a requirement to support in situ long-term observations on this issue. Over the past years, in situ seabed observation techniques have been developed, but technical challenges (e.g., deficiency of the sensor sensitivity and resolution) and the high cost of seafloor observations have largely limited the development of NLIW–seabed interaction studies. The limitations arise because the sensors have an inherent unpredictable drift, as well as the challenge of isolating NLIW signals from the other pressure/pore-pressure components. Short sharp signal shifts of pressure/pore pressure are easily captured, but small slow disturbances induced by NLIWs are more challenging. The precision and accuracy of sensors can likely be substantially improved in the future, for example, by using the correction factors that are usually applied when measuring surface waves with pressure sensors [97] to improvements in the continuous pressure-sensor monitoring of NLIW motions and improving the accuracy and resolution of the sensor measurements through advanced processing techniques, e.g., Kalman filtering or machine learning. We expect that the development of more advanced and lower-cost in situ seabed observation techniques will lead to more comprehensive monitoring of a wide range of NLIW–seabed interaction processes and the potential geohazards and environmental impacts that they trigger. Our understanding will be improved by these observational data, which will also help us better predict the response of the seabed dynamics to NLIW propagation on the continental slope.

Author Contributions: Conceptualization, T.C. and Y.J.; writing—original draft, T.C.; review and editing the article, Z.L., H.N., H.L. and H.S. All authors have read and agreed to the published version of the manuscript.

Funding: This work was supported by the Hainan Research Institute of China Engineering Science and Technology Development Strategy (No. 21-HN-ZD-02), the Open Research Fund of Key Laboratory of Coastal Science and Integrated Management, Ministry of Natural Resources (No. 2021COSIMQ007), the National Natural Science Foundation of China (No. 41831280), and the Fundamental Research Funds for the Central Universities (No. 202161039).

Institutional Review Board Statement: Not applicable.

Informed Consent Statement: Not applicable.

Data Availability Statement: No new data were created or analyzed in this study. Data sharing is not applicable to this article.

Acknowledgments: We are grateful to Zhihan Fan, Zhiwen Sun, and Liang Xue for their valuable comments and revisions to this review.

Conflicts of Interest: The authors declare no conflict of interest.

References

1. Cai, S.; Xie, J.; He, J. An overview of internal solitary waves in the South China Sea. *Surv. Geophys.* **2012**, *33*, 927–943. [[CrossRef](#)]

2. Boegman, L.; Stastna, M. Sediment resuspension and transport by internal solitary waves. *Annu. Rev. Fluid Mech.* **2019**, *51*, 129–154. [[CrossRef](#)]
3. Helfrich, K.R.; Melville, W.K. Long nonlinear internal waves. *Annu. Rev. Fluid Mech.* **2006**, *38*, 395–425. [[CrossRef](#)]
4. Stastna, M.; Coutino, A.; Walter, R.K. The effect of strong shear on internal solitary-like waves. *Nonlin. Process. Geophys.* **2021**, *28*, 585–598. [[CrossRef](#)]
5. Sarkar, S.; Scotti, A. From topographic internal gravity waves to turbulence. *Annu. Rev. Fluid Mech.* **2017**, *49*, 195–220. [[CrossRef](#)]
6. Lamb, K.G. Internal wave breaking and dissipation mechanisms on the continental slope/shelf. *Annu. Rev. Fluid Mech.* **2014**, *46*, 231–254. [[CrossRef](#)]
7. Moum, J.N.; Klymak, J.M.; Nash, J.D.; Perlin, A.; Smyth, W.D. Energy Transport by Nonlinear Internal Waves. *J. Phys. Oceanogr.* **2007**, *37*, 1968–1988. [[CrossRef](#)]
8. Chen, L.; Zheng, Q.; Xiong, X.; Yuan, Y.; Xie, H.; Guo, Y.; Yu, L.; Yun, S. Dynamic and Statistical Features of Internal Solitary Waves on the Continental Slope in the Northern South China Sea Derived from Mooring Observations. *J. Geophys. Res. Oceans* **2019**, *124*, 4078–4097. [[CrossRef](#)]
9. Li, D.; Chou, W.C.; Shih, Y.Y.; Chen, G.Y.; Chang, Y.; Chow, C.H.; Lin, T.Y.; Hung, C.C. Elevated particulate organic carbon export flux induced by internal waves in the oligotrophic northern South China Sea. *Sci. Rep.* **2018**, *8*, 2042. [[CrossRef](#)]
10. Magalhaes, J.M.; da Silva, J.C.B.; Buijsman, M.C. Long lived second mode internal solitary waves in the Andaman Sea. *Sci. Rep.* **2020**, *10*, 10234. [[CrossRef](#)]
11. Thomas, J.A.; Lerczak, J.A.; Moum, J.N. Horizontal variability of high-frequency nonlinear internal waves in Massachusetts Bay detected by an array of seafloor pressure sensors. *J. Geophys. Res. Oceans* **2016**, *121*, 5587–5607. [[CrossRef](#)]
12. Stöber, U.; Moum, J.N. On the potential for automated realtime detection of nonlinear internal waves from seafloor pressure measurements. *Appl. Ocean Res.* **2011**, *33*, 275–285. [[CrossRef](#)]
13. Jackson, C. Internal wave detection using the Moderate Resolution Imaging Spectroradiometer (MODIS). *J. Geophys. Res.* **2007**, *112*, 13. [[CrossRef](#)]
14. Tian, Z.; Liu, Y.; Zhang, X.; Zhang, Y.; Zhang, M. Formation Mechanisms and Characteristics of the Marine Nepheloid Layer: A Review. *Water* **2022**, *14*, 678. [[CrossRef](#)]
15. Huang, X.; Chen, Z.; Zhao, W.; Zhang, Z.; Zhou, C.; Yang, Q.; Tian, J. An extreme internal solitary wave event observed in the northern South China Sea. *Sci. Rep.* **2016**, *6*, 30041. [[CrossRef](#)]
16. Tian, Z.; Jia, Y.; Du, Q.; Zhang, S.; Guo, X.; Tian, W.; Zhang, M.; Song, L. Shearing stress of shoaling internal solitary waves over the slope. *Ocean Eng.* **2021**, *241*, 110046. [[CrossRef](#)]
17. Deepwell, D.; Sapède, R.; Buchart, L.; Swaters, G.E.; Sutherland, B.R. Particle transport and resuspension by shoaling internal solitary waves. *Phys. Rev. Fluids* **2020**, *5*, 054303. [[CrossRef](#)]
18. Edge, W.C.; Jones, N.L.; Rayson, M.D.; Ivey, G.N. Observations of enhanced sediment transport by nonlinear internal waves. *Geophys. Res. Lett.* **2020**, *47*, e2020GL088499.
19. Ma, X.; Yan, J.; Hou, Y.; Lin, F.; Zheng, X. Footprints of obliquely incident internal solitary waves and internal tides near the shelf break in the northern South China Sea. *J. Geophys. Res. Oceans* **2016**, *121*, 8706–8719. [[CrossRef](#)]
20. Van Haren, H. High-frequency bottom-pressure and acoustic variations in a sea strait: Internal wave turbulence. *Ocean Dyn.* **2012**, *62*, 1123–1137. [[CrossRef](#)]
21. Rivera-Rosario, G.A.; Diamessis, P.J.; Jenkins, J.T. Bed failure induced by internal solitary waves. *J. Geophys. Res. Oceans* **2017**, *122*, 5468–5485. [[CrossRef](#)]
22. Olsthoorn, J.; Stastna, M.; Soontiens, N. Fluid circulation and seepage in lake sediment due to propagating and trapped internal waves. *Water Resour. Res.* **2012**, *48*, W11520. [[CrossRef](#)]
23. Chen, C.Y.; Hsu, J.R.C. Interaction between internal waves and a permeable seabed. *Ocean. Eng.* **2005**, *32*, 587–621. [[CrossRef](#)]
24. Reeder, D.B.; Ma, B.B.; Yang, Y.J. Very large subaqueous sand dunes on the upper continental slope in the South China Sea generated by episodic, shoaling deep-water internal solitary waves. *Mar. Geol.* **2011**, *279*, 12–18. [[CrossRef](#)]
25. Huettel, M.; Berg, P.; Kostka, J.E. Benthic Exchange and Biogeochemical Cycling in Permeable Sediments. *Annu. Rev. Mar. Sci.* **2014**, *6*, 23–51. [[CrossRef](#)] [[PubMed](#)]
26. Rao, A.M.F.; McCarthy, M.J.; Gardner, W.S.; Jahnke, R.A. Respiration and denitrification in permeable continental shelf deposits on the South Atlantic Bight: N-2: Ar and isotope pairing measurements in sediment column experiments. *Cont. Shelf Res.* **2008**, *28*, 602–613. [[CrossRef](#)]
27. Lien, R.-C.; Henyey, F.; Ma, B.; Yang, Y.J. Large-Amplitude Internal Solitary Waves Observed in the Northern South China Sea: Properties and Energetics. *J. Phys. Oceanogr.* **2014**, *44*, 1095–1115. [[CrossRef](#)]
28. Edge, W.C.; Jones, N.L.; Rayson, M.D.; Ivey, G.N. Calibrated suspended sediment observations beneath large amplitude non-linear internal waves. *J. Geophys. Res. Oceans* **2021**, *126*, e2021JC017538. [[CrossRef](#)]
29. Miramontes, E.; Jouet, G.; Thereau, E.; Bruno, M.; Penven, P.; Guerin, C.; Le Roy, P.; Droz, L.; Jorry, S.J.; Hernández-Molina, F.J.; et al. The impact of internal waves on upper continental slopes: Insights from the Mozambican margin (southwest Indian Ocean). *Earth Surf. Process. Landf.* **2020**, *45*, 1469–1482. [[CrossRef](#)]
30. Zhang, W.; Didenkulova, I.; Kurkina, O.; Cui, Y.; Haberkern, J.; Aepfler, R.; Santos, A.I.; Zhang, H.; Hanebuth, T.J.J. Internal solitary waves control offshore extension of mud depocenters on the NW Iberian shelf. *Mar. Geol.* **2019**, *409*, 15–30. [[CrossRef](#)]

31. Guo, X.; Liu, Z.; Zheng, J.; Luo, Q.; Liu, X. Bearing capacity factors of T-bar from surficial to stable penetration into deep-sea sediments. *Soil Dyn. Earthq. Eng.* **2023**, *165*, 107671. [[CrossRef](#)]
32. Yamamoto, T.; Koning, H.L.; Sellmeijer, H.; Hijum, E.V. On the response of a poro-elastic bed to water waves. *J. Fluid Mech.* **1978**, *87*, 193–206. [[CrossRef](#)]
33. Anderson, D.; Cox, D.; Mieras, R.; Puleo, J.A.; Hsu, T.-J. Observations of wave-induced pore pressure gradients and bed level response on a surf zone sandbar. *J. Geophys. Res. Oceans* **2017**, *122*, 5169–5193. [[CrossRef](#)]
34. Sumer, B.M. Liquefaction around Marine structures. In *Coastal Structures 2007, Proceedings of the 5th Coastal Structures International Conference, CST07, Venice, Italy, 2–4 July 2009*; World Scientific Pub. Co.: Singapore, 2009; pp. 1864–1870.
35. Tian, Z.; Chen, T.; Yu, L.; Guo, X.; Jia, Y. Penetration depth of the dynamic response of seabed induced by internal solitary waves. *Appl. Ocean Res.* **2019**, *90*, 101867. [[CrossRef](#)]
36. Guo, X.; Stoesser, T.; Zheng, D.; Luo, Q.; Liu, X.; Nian, T. A methodology to predict the run-out distance of submarine landslides. *Comput. Geotech.* **2023**, *153*, 105073. [[CrossRef](#)]
37. Guo, X.; Nian, T.; Fu, C.; Zheng, D. Numerical Investigation of the Landslide Cover Thickness Effect on the Drag Forces Acting on Submarine Pipelines. *J. Waterw. Port Coast. Ocean Eng.* **2023**, *149*, 04022032. [[CrossRef](#)]
38. Sultan, N.; Murphy, S.; Riboulot, V.; Géli, L. Creep-dilatancy development at a transform plate boundary. *Nat. Commun.* **2022**, *13*, 1913. [[CrossRef](#)]
39. Lai, J.; Richards, A.; Keller, G. In Place Measurement of Excess Pore Pressure in Gulf of Maine Clays. In *Transactions-American Geophysical Union*; American Geophysical Union: Washington, DC, USA, 1968; p. 221.
40. Richards, A.F.; Øten, K.; Keller, G.H.; Lai, J.Y. Differential piezometer probe for an in situ measurement of sea-floor. *Geotechnique* **1975**, *25*, 229–238. [[CrossRef](#)]
41. Lamb, K.G.; Warn-Varnas, A. Two-dimensional numerical simulations of shoaling internal solitary waves at the ASIAEX site in the South China Sea. *Nonlin. Process. Geophys.* **2015**, *22*, 289–312. [[CrossRef](#)]
42. Xie, J.; He, Y.; Cai, S. Bumpy Topographic Effects on the Transbasin Evolution of Large-Amplitude Internal Solitary Wave in the Northern South China Sea. *J. Geophys. Res. Oceans* **2019**, *124*, 4677–4695. [[CrossRef](#)]
43. Moum, J.N.; Nash, J.D. Seafloor Pressure Measurements of Nonlinear Internal Waves. *J. Phys. Oceanogr.* **2008**, *38*, 481–491. [[CrossRef](#)]
44. Liu, T.; Wei, G.; Kou, H.; Guo, L. Pore pressure observation: Pressure response of probe penetration and tides. *Acta Oceanol. Sin.* **2019**, *38*, 107–113. [[CrossRef](#)]
45. Higashino, M.; Clark, J.J.; Stefan, H.G. Pore water flow due to near-bed turbulence and associated solute transfer in a stream or lake sediment bed. *Water Resour. Res.* **2009**, *45*, W12414. [[CrossRef](#)]
46. Moum, J.N.; Smyth, W.D. The pressure disturbance of a nonlinear internal wave train. *J. Fluid Mech.* **2006**, *558*, 153–177. [[CrossRef](#)]
47. Williams, S.J.; Jeng, D.S. The effects of a porous-elastic seabed on interfacial wave propagation. *Ocean Eng.* **2007**, *34*, 1818–1831. [[CrossRef](#)]
48. Hsu, J.R.C.; Jeng, D.S.; Tsai, C.P. Short-crested wave-induced soil response in a porous seabed of infinite thickness. *Int. J. Numer. Anal. Methods Geomech.* **1993**, *17*, 553–576. [[CrossRef](#)]
49. Forgia, G.I.; Sciortino, G. The role of the free surface on interfacial solitary waves. *Phys. Fluids* **2019**, *31*, 106601. [[CrossRef](#)]
50. Kodaira, T.; Waseda, T.; Miyata, M.; Choi, W. Internal solitary waves in a two-fluid system with a free surface. *J. Fluid Mech.* **2016**, *804*, 201–223. [[CrossRef](#)]
51. Zhi, C.; Wang, H.; Chen, K.; You, Y. Theoretical and experimental investigation on strongly nonlinear internal solitary waves moving over slope-shelf topography. *Ocean Eng.* **2021**, *223*, 108645. [[CrossRef](#)]
52. Apel, J.R.; Ostrovsky, L.A.; Stepanyants, Y.A.; Lynch, J.F. Internal solitons in the ocean and their effect on underwater sound. *J. Acoust. Soc. Am.* **2007**, *121*, 695–722. [[CrossRef](#)]
53. Van Haren, H. Bottom-pressure observations of deep-sea internal hydrostatic and non-hydrostatic motions. *J. Fluid Mech.* **2013**, *714*, 591–611. [[CrossRef](#)]
54. Yang, Y.J.; Lien, R.-C.; Chang, M.-H.; Tang, T.Y. *Pressure Perturbations Induced by Mode-1 Depression Internal Solitary Waves*; European Geosciences Union General Assembly: Vienna, Austria, 2011.
55. Fukao, Y.; Miyama, T.; Tono, Y.; Sugioka, H.; Ito, A.; Shiobara, H.; Yamashita, M.; Varlamov, S.; Furue, R.; Miyazawa, Y. Detection of ocean internal tide source oscillations on the slope of Aogashima Island, Japan. *J. Geophys. Res. Oceans* **2019**, *124*, 4918–4933. [[CrossRef](#)]
56. Saito, T.; Tsushima, H. Synthesizing ocean bottom pressure records including seismic wave and tsunami contributions: Toward realistic tests of monitoring systems. *J. Geophys. Res. Solid Earth* **2016**, *121*, 8175–8195. [[CrossRef](#)]
57. Deng, H.; An, C.; Cai, C.; Ren, H. Theoretical Solution and Applications of Ocean Bottom Pressure Induced by Seismic Waves at High Frequencies. *Geophys. Res. Lett.* **2022**, *49*, e2021GL096952. [[CrossRef](#)]
58. Watts, D.R.; Wei, M.; Tracey, K.L.; Donohue, K.A.; He, B. Seafloor Geodetic Pressure Measurements to Detect Shallow Slow Slip Events: Methods to Remove Contributions from Ocean Water. *J. Geophys. Res. Solid Earth* **2021**, *126*, e2020JB020065. [[CrossRef](#)]
59. Van Haren, H. Internal wave–turbulence pressure above sloping sea bottoms. *J. Geophys. Res. Oceans* **2011**, *116*, C12004. [[CrossRef](#)]
60. Schultheiss, P.J. Pore pressures in marine sediments: An overview of measurement techniques and some geological and engineering applications. *Mar. Geophys. Res.* **1990**, *12*, 153–168. [[CrossRef](#)]
61. Jeng, D.S. *Porous Models for Wave-Seabed Interactions*; Springer: Berlin/Heidelberg, Germany, 2012.
62. Jeng, D.-S. *Mechanics of Wave-Seabed-Structure Interactions: Modelling, Processes and Applications*; Cambridge University Press: Cambridge, UK, 2018.
63. Biot, M.A. General Theory of Three-Dimensional Consolidation. *J. Appl. Phys.* **1941**, *12*, 155–164. [[CrossRef](#)]

64. Verruijt, A. Elastic Storage of Aquifers. In *Flow through Porous Media*; Wiest, R.J.M.D., Ed.; Academic Press: New York, NY, USA, 1969; pp. 331–376.
65. Williams, S.; Jeng, D. Viscous attenuation of interfacial waves over a porous seabed. *J. Coast. Res.* **2007**, *50*, 338–342.
66. Bear, J. *Dynamics of Fluids in Porous Media*; Courier Corporation: Chelmsford, MA, USA, 2013.
67. Qiao, L.; Guo, X.; Tian, Z.; Yu, L. Experimental analysis of pore pressure characteristics of slope sediments by shoaling internal solitary waves. *Acta Oceanol. Sin.* **2018**, *40*, 68–76.
68. Gong, Y.; Song, H.; Zhao, Z.; Guan, Y.; Zhang, K.; Kuang, Y.; Fan, W. Enhanced diapycnal mixing with polarity-reversing internal solitary waves revealed by seismic reflection data. *Nonlin. Process. Geophys.* **2021**, *28*, 445–465. [[CrossRef](#)]
69. Shroyer, E.L.; Moum, J.N.; Nash, J.D. Observations of Polarity Reversal in Shoaling Nonlinear Internal Waves. *J. Phys. Oceanogr.* **2009**, *39*, 691–701. [[CrossRef](#)]
70. Orr, M.H. Nonlinear internal waves in the South China Sea: Observation of the conversion of depression internal waves to elevation internal waves. *J. Geophys. Res.* **2003**, *108*, 16. [[CrossRef](#)]
71. Li, Y.; Liu, L.; Gao, S.; Zhang, Y.; Xiong, X. Experimental study on dynamic response characteristics of continental shelf slope to internal solitary waves. *Acta Oceanol. Sin.* **2021**, *43*, 126–134.
72. Lynch, J.F.; Ramp, S.R.; Ching-Sang, C.; Tswen Yung, T.; Yang, Y.J.; Simmen, J.A. Research highlights from the Asian Seas International Acoustics Experiment in the South China Sea. *IEEE J. Ocean. Eng.* **2004**, *29*, 1067–1074. [[CrossRef](#)]
73. Klymak, J.M.; Moum, J.N. Internal solitary waves of elevation advancing on a shoaling shelf. *Geophys. Res. Lett.* **2003**, *30*, 2045. [[CrossRef](#)]
74. Madsen, O.S. Stability of a Sand Bed under Breaking Waves. In Proceedings of the 14th International Conference on Coastal Engineering, Copenhagen, Denmark, 24–28 June 1974; pp. 776–794.
75. Liu, P.L.F.; Park, Y.S.; Lara, J.L. Long-wave-induced flows in an unsaturated permeable seabed. *J. Fluid Mech.* **2007**, *586*, 323–345. [[CrossRef](#)]
76. Torum, A. Wave-induced pore pressures—Air/gas content. *J. Waterw. Port Coast. Ocean Eng. ASCE* **2007**, *133*, 83–86. [[CrossRef](#)]
77. Cross, R.H.; Baker, V.A.; Treadwell, D.D.; Huntsman, S. Attenuation of Wave-Induced Pore Pressures in Sand. In *Civil Engineering in the Oceans IV*; ASCE: Reston, VA, USA, 1979.
78. Bennett, R.H.; Faris, J.R. Ambient and dynamic pore pressures in fine-grained submarine sediments: Mississippi Delta. *Appl. Ocean Res.* **1979**, *1*, 115–123. [[CrossRef](#)]
79. Jin, G.; Tang, H.; Gibbes, B.; Li, L.; Barry, D.A. Transport of nonsorbing solutes in a streambed with periodic bedforms. *Adv. Water Resour.* **2010**, *33*, 1402–1416. [[CrossRef](#)]
80. Elliott, A.H.; Brooks, N.H. Transfer of nonsorbing solutes to a streambed with bed forms: Theory. *Water Resour. Res.* **1997**, *33*, 123–136. [[CrossRef](#)]
81. Bear, J. *Modeling Phenomena of Flow and Transport in Porous Media*; Springer: Cham, Switzerland, 2018.
82. Huettel, M.; Ziebis, W.; Forster, S. Flow-induced uptake of particulate matter in permeable sediments. *Limnol. Oceanogr.* **1996**, *41*, 309–322. [[CrossRef](#)]
83. Boegman, L.; Ivey, G.N. Flow separation and resuspension beneath shoaling nonlinear internal waves. *J. Geophys. Res. Oceans* **2009**, *114*, C02018. [[CrossRef](#)]
84. Quaresma, L.S.; Vitorino, J.; Oliveira, A.; da Silva, J. Evidence of sediment resuspension by nonlinear internal waves on the western Portuguese mid-shelf. *Mar. Geol.* **2007**, *246*, 123–143. [[CrossRef](#)]
85. Hosegood, P.; van Haren, H. Near-bed solibores over the continental slope in the Faeroe-Shetland Channel. *Deep Sea Res. Part II Top. Stud. Oceanogr.* **2004**, *51*, 2943–2971. [[CrossRef](#)]
86. Bogucki, D.; Dickey, T.; Redekopp, L.G. Sediment Resuspension and Mixing by Resonantly Generated Internal Solitary Waves. *J. Phys. Oceanogr.* **1997**, *27*, 1181–1196. [[CrossRef](#)]
87. Johnson, D.R.; Weidemann, A.; Pegau, W.S. Internal tidal bores and bottom nepheloid layers. *Cont. Shelf Res.* **2001**, *21*, 1473–1484. [[CrossRef](#)]
88. Bluteau, C.E.; Smith, S.L.; Ivey, G.N.; Schlosser, T.L.; Jones, N.L. Assessing the relationship between bed shear stress estimates and observations of sediment resuspension in the ocean. In Proceedings of the 20th Australasian Fluid Mechanics Conference, Perth, Australia, 5–8 December 2016.
89. Aghsaee, P.; Boegman, L. Experimental investigation of sediment resuspension beneath internal solitary waves of depression. *J. Geophys. Res. Oceans* **2015**, *120*, 3301–3314. [[CrossRef](#)]
90. Richards, C.; Bourgault, D.; Galbraith, P.S.; Hay, A.; Kelley, D.E. Measurements of shoaling internal waves and turbulence in an estuary. *J. Geophys. Res. Oceans* **2013**, *118*, 273–286. [[CrossRef](#)]
91. Aghsaee, P.; Boegman, L.; Diamessis, P.J.; Lamb, K.G. Boundary-layer-separation-driven vortex shedding beneath internal solitary waves of depression. *J. Fluid Mech.* **2012**, *690*, 321–344. [[CrossRef](#)]
92. Droghei, R.; Falcini, F.; Casalbore, D.; Martorelli, E.; Mosetti, R.; Sannino, G.; Santoleri, R.; Chiocci, F.L. The role of Internal Solitary Waves on deep-water sedimentary processes: The case of up-slope migrating sediment waves off the Messina Strait. *Sci. Rep.* **2016**, *6*, 36376. [[CrossRef](#)] [[PubMed](#)]
93. Cheng, M.-H.; Hsieh, C.-M.; Hsu, J.R.C.; Hwang, R.R. Effect of porosity on an internal solitary wave propagating over a porous trapezoidal obstacle. *Ocean Eng.* **2017**, *130*, 126–141. [[CrossRef](#)]

94. Lamb, K.G.; Xiao, W. Internal solitary waves shoaling onto a shelf: Comparisons of weakly-nonlinear and fully nonlinear models for hyperbolic-tangent stratifications. *Ocean Model.* **2014**, *78*, 17–34. [[CrossRef](#)]
95. Santos, I.R.; Eyre, B.D.; Huettel, M. The driving forces of porewater and groundwater flow in permeable coastal sediments: A review. *Estuar. Coast. Shelf Sci.* **2012**, *98*, 1–15. [[CrossRef](#)]
96. Bourgault, D.; Morsilli, M.; Richards, C.; Neumeier, U.; Kelley, D.E. Sediment resuspension and nepheloid layers induced by long internal solitary waves shoaling orthogonally on uniform slopes. *Cont. Shelf Res.* **2014**, *72*, 21–33. [[CrossRef](#)]
97. Marino, M.; Rabionet, I.C.; Musumeci, R.E. Measuring free surface elevation of shoaling waves with pressure transducers. *Cont. Shelf Res.* **2022**, *245*, 104803. [[CrossRef](#)]

Disclaimer/Publisher’s Note: The statements, opinions and data contained in all publications are solely those of the individual author(s) and contributor(s) and not of MDPI and/or the editor(s). MDPI and/or the editor(s) disclaim responsibility for any injury to people or property resulting from any ideas, methods, instructions or products referred to in the content.